Multiscale analysis of mixed-mode fracture and effective traction-separation relations for composite materials

Turteltaub, Sergio; van Hoorn, Niels; Westbroek, Wim; Hirsch, Christian

DOI
10.1016/j.jmps.2018.04.009

Publication date
2018

Document Version
Accepted author manuscript

Published in
Journal of the Mechanics and Physics of Solids

Citation (APA)
Turteltaub, S., van Hoorn, N., Westbroek, W., & Hirsch, C. (2018). Multiscale analysis of mixed-mode fracture and effective traction-separation relations for composite materials. *Journal of the Mechanics and Physics of Solids*, *117*, 88-109. https://doi.org/10.1016/j.jmps.2018.04.009

Multiscale analysis of mixed-mode fracture and effective traction-separation relations for composite materials

Sergio Turteltaub[a,*], Niels van Hoorn[a], Wim Westbroek[a], Christian Hirsch[b]

[a]*Delft University of Technology, Faculty of Aerospace Engineering, Kluyverweg 1, 2629 HS Delft, The Netherlands*
[b]*Technische Universität Dresden, Faculty of Mechanical Science and Engineering, 01062 Dresden, Germany*

Abstract

A multiscale framework for the analysis of fracture is developed in order to determine the effective (homogenized) strength and fracture energy of a composite material based on the constituent's material properties and microstructural arrangement. The method is able to deal with general (mixed-mode) applied strains without a priori knowledge of the orientation of the cracks. Cracks occurring in a microscopic volume element are modeled as sharp interfaces governed by microscale traction-separation relations, including interfaces between material phases to account for possible microscale debonding. Periodic boundary conditions are used in the microscopic volume element, including periodicity that allows cracks to transverse the boundaries of the volume element at arbitrary orientations. A kinematical analysis is presented for the proper interpretation of a periodic microscopic crack as an equivalent macroscopic periodic crack in a single effective orientation. It is shown that the equivalent crack is unaffected by the presence of parallel periodic replicas, hence providing the required information of a single localized macroscopic crack. A strain decomposition in the microscopic volume element is used to separate the contributions from the crack and the surrounding bulk material. Similarly, the (global) Hill-Mandel condition for the volume element is separated into a bulk-averaged condition and a crack-averaged condition. Further, it is shown that, though the global Hill-Mandel condition can be satisfied a priori using periodic boundary conditions, the crack-based condition can be used to actually determine the effective traction of an equivalent macroscopic crack.

Keywords:
multiscale fracture, cohesive elements, representative volume element, Hill-Mandel relation

1. Introduction

Prediction of the onset and evolution of failure in composite materials such as fiber-reinforced composites is an essential factor in the design and development of load-bearing components used in lightweight structures. While significant progress has been achieved in this area since the transportation industry embraced the use of composites, there is a need to further refine the predictability and robustness of models used to analyze failure. Current safety factors used in design of

*Corresponding author
Email address: S.R.Turteltaub@tudelft.nl (Sergio Turteltaub)

structures made of composite materials significantly limit their efficiency due to large uncertainties. Multiscale methods offer the possibility of incorporating detailed information of a composite, which should lead to an improvement in accuracy of failure models. Equally important is the need to develop models that predict the evolution of failure in composites, which is relevant in order to determine the residual structural strength after (partial) failure or to design a structure against a catastrophic event (e.g., impact).

In recent years, the use of cohesive laws, in conjunction with either cohesive elements or with the extended finite element method (XFEM) has gained popularity as a tool to simulate the onset and propagation of cracks in composite materials. Nevertheless, establishing reliable cohesive laws for composite materials remains challenging, particularly regarding the incorporation of lower length scale information at a higher length scale. The determination of a macroscopic cohesive relation, which accounts for microscale features and fracture mechanisms, relies on a homogenization approach that translates the detailed behavior in a microstructural volume element into an effective (macroscale) response. For multiscale formulations involving fracture, the classical notion of a representative volume element (RVE) that is based on a continuous displacement requires a modification (see, e.g., Gitman et al. (2007)). An alternative averaging formulation based on a damaged zone within the volume element was proposed by Nguyen et al. (2010) where it was concluded that with a proper identification an RVE can be established.

Multiscale formulations have been applied to the so-called adhesive cracks, in which it is a priori known in what region and, more importantly, in what orientation a macroscopic crack is expected to nucleate and grow (Verhoosel et al., 2010; Matous et al., 2008; Kulkarni et al., 2010). Micromechanical formulations have been used to study failure in polymer composites using periodic boundary conditions in Melro et al. (2013) where the influence of the distinct material and interface properties were analyzed. Similarly, the influence of defects on the strength and fracture energy of a fiber-reinforced unidirectional composite under extension was analyzed in Alfaro et al. (2010a) where it was observed that imperfections may increase the effective crack length compared to the crack length in a sample without imperfections, thus actually increasing the macroscopic fracture energy. In-plane periodic conditions where used to analyze the response of one ply in Arteiro et al. (2014), with elastic adjacent plies preventing out-of-plane crack propagation beyond the ply analyzed (i.e., a so-called "wall effect" as described in Gitman et al. (2007)). Their simulations provide insight on the interplay between ply geometry and properties, constraining effects of adjacent plies and the resulting crack patterns.

One issue that has been identified as a potential problem is related to the strong (i.e., pointwise) periodic boundary conditions and its effect on the results. To overcome the limitation of having to prescribe a priori the orientation of a crack (i.e., analysis limited to adhesive cracks) and simultaneously to address some doubts that have been raised about the suitability of strong periodic boundary conditions to analyze fracture, a multiscale transition scheme was proposed in which the representative volume element is, upon the onset of cracking (localization of damage), replaced by a microstructural volume element (MVE) (Coenen et al., 2012a,b; Bosco et al., 2015). Through a continuous adaptation of the loading at the microscale level, using the so-called percolation-path-aligned boundary conditions, the MVE provides a macroscopic response aligned with the average orientation of the crack as it develops throughout the loading process. Their scheme was implemented in a so-called FE^2 framework, where numerical simulations are simul-

taneously conducted at the micro and macroscales. Also addressing the issue of strong periodic boundary conditions, an alternative approach pertaining to weakly periodic boundary conditions has been recently developed (Svenning et al., 2016a,b). These conditions lead to a mixed traction-displacement formulation as unknowns in the boundary.

The FE^2 approach requires continuous bi-directional exchange of information between the macroscale and the microscale domains throughout a simulation Mosby and Matous (2016). In a displacement-driven multiscale formulation, a macroscale strain increment is given as input to an RVE (in undamaged zones) or to an MVE (in damaged areas) and the corresponding microscale boundary value problem is solved, which explicitly accounts for microstructural phenomena. Subsequently, the averaged microscale response is provided as input to the macroscale boundary value problem, typically in the form of an average (macroscopic) stress increment, a tangent (value of derivative of stress with respect to a strain measure) and possibly some variables that are treated as internal parameters at the macroscale. In this approach, the constitutive information at the macroscale is not specified in closed-form (or with a system of equations) but rather in implicit form through the (incremental) solution of microscale boundary value problems, one for each macroscale integration point in a finite element formulation.

An alternative approach, which is attractive from the point of view of computational efficiency, is to propose a macroscopic model in closed-form and use MVEs to essentially calibrate the constitutive information a priori (i.e., the parameters in the macroscopic model are chosen to approximate the explicit MVE results). The clear advantage is that it is possible to carry out a single-scale computation while retaining relevant information about the microscale phenomena. One limitation of this approach is that the macroscopic model may not be able to reproduce all possible responses from the MVE calculation, particularly for complex loading histories. Nonetheless, accurate results may be expected for simpler loading cases (e.g., locally proportional loading), which can still reproduce a relatively complex macroscopic loading case.

Within the context of computational efficiency, the present work addresses two issues in a hierarchical multiscale framework for fracture: (i) the suitability of strong periodic boundary conditions under relatively general loading conditions and (ii) a methodology to establish a macroscopic cohesive law that implicitly incorporates microscopic information. For the first issue, an analysis is carried out to introduce the notion of an "equivalent crack domain", where it is shown that the response after localization due to fracture under strong periodic boundary conditions can be described by a single equivalent crack and is independent of parallel crack replicas. The method relies on a description of fracture at the microscale level based on crack surfaces (as opposed to distributed damage theories that simulate cracking in a region). In practice this simplifies the numerical implementation since only one type of fracture model is required. Furthermore, the crack surface approach can still be used in conjunction with a distributed model for, e.g., plasticity. Through representative simulations it is verified that the periodic boundary conditions provide sufficient freedom to allow cracks to nucleate in arbitrary orientations. Hence, one criticism of periodic boundary conditions is addressed and the theoretical framework provides a simple and computationally-efficient method to impose boundary conditions for fracture problems. For the second issue mentioned above, the present work indicates the steps required to derive a macroscopic cohesive relation that, through interpolation of data generated parametrically from representative loading cases, can be used for a wider range of loading conditions (i.e., arbitrary mixed-

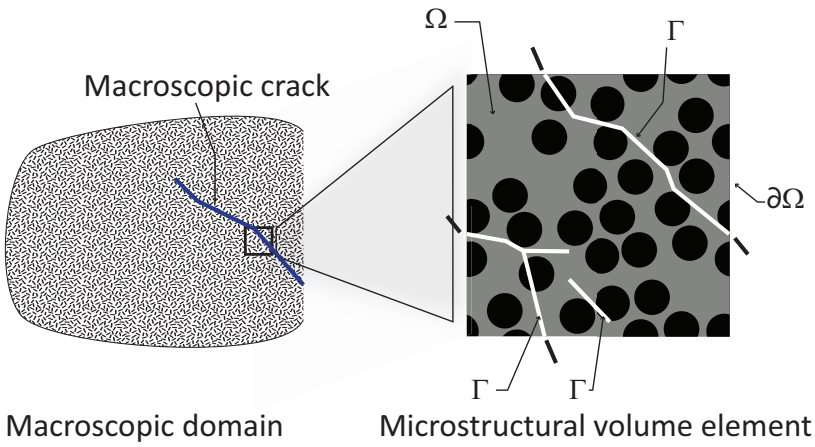

Figure 1: Microstructural volume element representing a cross-section perpendicular to the fiber direction of an unidirectional fiber-reinforced composite.

mode loading conditions). An analysis of the Hill-Mandel conditions in the context of periodic boundary conditions is carried out. The expressions of the effective quantities that describe a macrocrack are derived from this analysis, which can be used in the description of the kinematic and kinetic aspects of a macroscopic cohesive relation for a composite material.

The paper is organized as follows: In Sec. 2 the microscale problem with periodic boundary conditions is formulated. The scale transition relations are discussed in Sec. 3. Quantities associated with an equivalent macroscopic crack are defined in Sec. 4. This section includes an interpretation of the Hill-Mandel conditions for an equivalent crack and the general form of a macroscopic traction-separation (cohesive) relation for a composite material. An analysis to (numerically) verify the scale transition requirements in terms of a crack-based Hill-Mandel condition is presented in Sec. 5. The existence of a representative volume element for fracture is studied in Sec. 6 for various loading cases. Based on the representative elements, macroscopic fracture data is summarized in Sec. 7 to illustrate the general procedure to create a material database from simulations. Concluding remarks are given in Sec. 8.

2. Microscale formulation

In a hierarchical multiscale formulation, a material point in a macroscopic domain represents the collective (or effective) behavior of a microstructural volume element. For simplicity, attention is limited here to a two-dimensional volume element that represents a cross-section of a composite as illustrated in Fig. 1 (for example, a cross-section perpendicular to the fiber direction of an unidirectional fiber-reinforced composite). Extensions to the three-dimensional case are also indicated whenever appropriate. The approach adopted is as follows: a nominal (macroscopic) deformation is applied to a volume element containing microscale information. Lower length scale information is given through phase-specific cohesive relations (e.g., separate cohesive relations for fibers, matrix and also for fiber-matrix interfaces in a fiber-reinforced composite). Subsequently, the fracture process inside the volume element is modeled until the specimen fails (i,e., it can no longer transmit a load). The microscale information is then post-processed to extract an effective

macroscopic traction-separation relation applicable for the given nominal deformation. The "calibrated" traction-separation relation can be subsequently used to model a fracture process at the macroscopic scale without the need to explicitly model the microscale phenomena. The method is intended for a sufficiently thick specimen in the cross-sectional plane although it can be adapted to account for so-called "wall-effects". This extension, however, is beyond the scope of the present work.

The procedure to calibrate a macroscopic traction-separation relation requires solving a series of boundary value problem on microstructural volume elements. In order to relate the microscale information to the macroscale behavior, a scale transition relation is required. The guiding principle is that the total energy dissipated due to the microscale fracture process should coincide with the macroscopic dissipation of an equivalent traction-separation relation, in line with the Hill-Mandel condition (Verhoosel et al., 2010; Hill, 1972, 1985). In a multiscale formulation where the displacement field remains continuous , the macroscopic stress and strain tensors are viewed as (weighted) averages of their microscopic counterparts, with an average performed in a representative volume element (RVE). If fracture occurs, however, the volume average cannot be used in its traditional form due to the displacement discontinuity associated to cracks. Instead, one has to consider a version of the divergence theorem that includes jumps along surfaces of discontinuity within the volume element (see, e.g., (Unger, 2013)).

In the present work, strong periodic boundary conditions are applied to a microstructural volume element in all space directions. There have been issues raised in the literature about the suitability of pointwise periodic boundary conditions in the context of fracture, hence a discussion on the Hill-Mandel requirement for the micro- to macro-scale transition in the context of periodicity as well as the geometrical interpretation of periodic cracks is pertinent.

As shown in Fig. 1, denote as Ω the microstructural volume element, $\partial\Omega$ as the external boundary of the microstructural volume element and Γ as the line (in two-dimensions) or surface (in three-dimensions) where a crack appears in the microstructural volume element. For simplicity, in the two-dimensional case, the domain is taken as a $l_1 \times l_2$ rectangular domain with corner nodes denoted as $\boldsymbol{x}^{(i)}$, $i = 1, 2, 3, 4$, and the boundary $\partial\Omega$ is divided into four sides denoted as $\partial\Omega_i$, $i = 1, 2, 3, 4$ as shown in Fig. 2. The outward unit vector to $\partial\Omega$ is denoted as $\boldsymbol{n}$ in general, while the specific outward unit vector to a side $\partial\Omega_i$ is denoted as $\boldsymbol{n}_i$, with $i = 1, 2, 3, 4$. The normal vector to the crack surface Γ is denoted as $\boldsymbol{m}$, with the convention that $\boldsymbol{m} = \boldsymbol{m}^-$ is the vector pointing towards the Γ^+ side while $\boldsymbol{m}^+ = -\boldsymbol{m}^-$ is the vector pointing towards the Γ^- side (see inset in Fig. 2). The choice of the + and - sides for Γ is in principle arbitrary (similar to a sign convention) but it needs to be consistently interpreted, particularly when computing integrals along the crack surface. For convenience, a global Cartesian basis $\boldsymbol{e}_1, \boldsymbol{e}_2$ is chosen such that $\boldsymbol{e}_1 = \boldsymbol{n}_1$ and $\boldsymbol{e}_2 = \boldsymbol{n}_2$. The crack Γ may represent a collection of disconnected crack segments, with possible bifurcations. Due to periodicity, some seemingly disconnected segments represent in fact a continuous crack (i.e., the crack leaves and re-enters periodically the volume element at periodically-connected points on $\partial\Omega$). A discussion on the geometrical interpretation of periodic cracks is given in Appendix A.

The crack surface Γ is in general not known a priori but, rather, it is obtained as the outcome of a simulation. Unless otherwise indicated, Γ refers to the cracked state of a *fully-failed* volume element, although some isolated and partially-failed segments of Γ may still be able to transmit loads at the end of the simulation. Central to the present formulation is that cracks are allowed

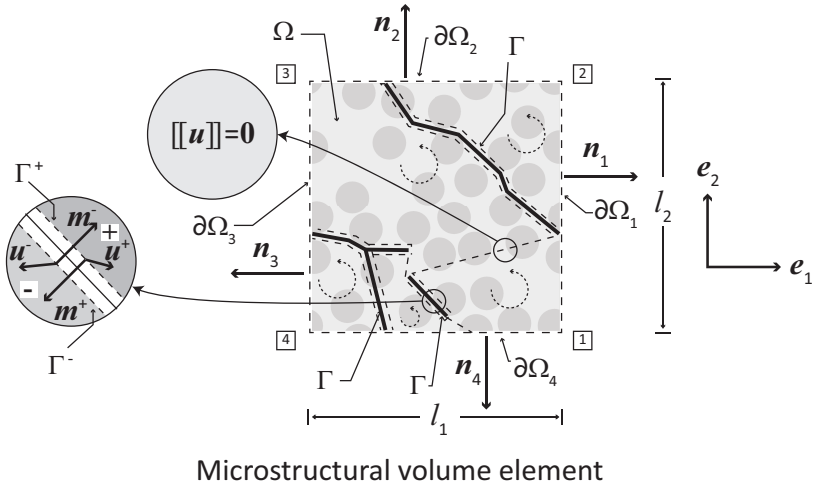

Figure 2: Nomenclature used in the two-dimensional rectangular volume element and decomposition of the microscopic domain Ω into subdomains with boundaries (dashed lines) that contain the external boundary $\partial\Omega$, the crack surface Γ and possibly uncracked parts of the material where the displacement is continuous. Line integrals in the subdomains are by convention performed in an anti-clockwise fashion.

to cross the external boundaries at arbitrary locations, albeit periodically. To this end, periodic boundary conditions are applied separately to both sides of points where a crack may cross the external boundary of the domain.

The microscale boundary-value problem for a quasi-static process with a crack Γ and with periodic boundary conditions is, in the absence of body forces, as follows:

$$\begin{cases} \operatorname{div}\boldsymbol{\sigma}(\boldsymbol{x},t) = \boldsymbol{0} & & \boldsymbol{x} \text{ in } \Omega \setminus \Gamma \\ \boldsymbol{t}^+(\boldsymbol{x}^+,t) = -\boldsymbol{t}^-(\boldsymbol{x}^-,t) & & \boldsymbol{x} \text{ on } \Gamma \\ \boldsymbol{u}(\boldsymbol{x}+l_1\boldsymbol{e}_1,t) - \boldsymbol{u}(\boldsymbol{x},t) = l_1\overline{\boldsymbol{\epsilon}}(t)\boldsymbol{e}_1 & \boldsymbol{t}(\boldsymbol{x}+l_1\boldsymbol{e}_1,t) = -\boldsymbol{t}(\boldsymbol{x},t) & \boldsymbol{x} \text{ on } \partial\Omega_3 \setminus \Gamma \\ \boldsymbol{u}(\boldsymbol{x}+l_2\boldsymbol{e}_2,t) - \boldsymbol{u}(\boldsymbol{x},t) = l_2\overline{\boldsymbol{\epsilon}}(t)\boldsymbol{e}_2 & \boldsymbol{t}(\boldsymbol{x}+l_2\boldsymbol{e}_2,t) = -\boldsymbol{t}(\boldsymbol{x},t) & \boldsymbol{x} \text{ on } \partial\Omega_4 \setminus \Gamma \\ \boldsymbol{u}^\pm(\boldsymbol{x}^\pm+l_1\boldsymbol{e}_1,t) - \boldsymbol{u}^\pm(\boldsymbol{x}^\pm,t) = l_1\overline{\boldsymbol{\epsilon}}(t)\boldsymbol{e}_1 & \boldsymbol{t}^\pm(\boldsymbol{x}^\pm+l_1\boldsymbol{e}_1,t) = -\boldsymbol{t}^\pm(\boldsymbol{x}^\pm,t) & \boldsymbol{x} \text{ on } \partial\Omega_3 \cap \Gamma \\ \boldsymbol{u}^\pm(\boldsymbol{x}^\pm+l_2\boldsymbol{e}_2,t) - \boldsymbol{u}^\pm(\boldsymbol{x}^\pm,t) = l_2\overline{\boldsymbol{\epsilon}}(t)\boldsymbol{e}_2 & \boldsymbol{t}^\pm(\boldsymbol{x}^\pm+l_2\boldsymbol{e}_2,t) = -\boldsymbol{t}^\pm(\boldsymbol{x}^\pm,t) & \boldsymbol{x} \text{ on } \partial\Omega_4 \cap \Gamma \end{cases} \tag{1}$$

where $\boldsymbol{\sigma}$ is the stress tensor, div is the divergence operator, $\boldsymbol{t}$ is the traction vector acting on the corresponding surface (Γ or $\partial\Omega$), $\boldsymbol{u}$ is the displacement vector and $\overline{\boldsymbol{\epsilon}} = \overline{\boldsymbol{\epsilon}}(t)$ corresponds to a prescribed macroscopic strain tensor applied on the volume element that drives the deformation process at different times t. The set $\Omega \setminus \Gamma$ refers to points in the bulk, uncracked material while $\partial\Omega \cap \Gamma$ refers to the points where the crack crosses the external boundary of the domain. The superscripts + and - refer to values on opposites sides of the surface Γ. The tractions $\boldsymbol{t}^\pm$ for points on the intersection between Γ and $\partial\Omega$ are computed with respect to the corresponding *outward* normal vector of $\partial\Omega$. It is noted that the points where a crack crosses the boundary domain are not known a priori but, rather, they are identified as they appear during the loading. For implementation purposes in a displacement-driven numerical solution, the displacement of the corner nodes in the rectangular domain can be specified as $\boldsymbol{u}(\boldsymbol{x}^{(i)},t) = \overline{\boldsymbol{\epsilon}}(t)\boldsymbol{x}^{(i)}$, with $i = 1,2,3,4$,

while the displacements of all the other boundary points are subjected to the periodicity conditions. In view of this, care must be exercised interpreting the results since the domain Ω may contain *multiple* parallel cracks and/or (finite) crack branches and/or isolated crack segments. A procedure to extract the information for a periodic crack is developed in the sequel.

At regular points $\boldsymbol{x}$ that are not on the crack surface, the displacement and strain fields are related as

$$\boldsymbol{\epsilon} = \frac{1}{2}\left(\nabla \boldsymbol{u} + \nabla \boldsymbol{u}^{\mathrm{T}}\right) \qquad \boldsymbol{x} \in \Omega \setminus \Gamma\,, \tag{2}$$

where the superscript T refers to the transpose. For a composite made out of linearly elastic and brittle solid phases, the constitutive relation at regular points is given by $\boldsymbol{\sigma} = \mathbb{C}\boldsymbol{\epsilon} \quad \boldsymbol{x}$ in $\Omega \setminus \Gamma$ where $\mathbb{C} = \mathbb{C}(\boldsymbol{x})$ represents the stiffness tensor at point $\boldsymbol{x}$ (e.g., either matrix or fiber). The present formulation is not restricted to brittle elastic materials but for simplicity this constitutive model will be used in the simulations. At points on the crack surface Γ, the constitutive response is taken as

$$\boldsymbol{t} = \boldsymbol{f}_{\mathrm{coh}}\left(\llbracket \boldsymbol{u} \rrbracket, \boldsymbol{\kappa}, \boldsymbol{m}\right) \qquad \boldsymbol{x} \text{ in } \Gamma$$

where $\boldsymbol{f}_{\mathrm{coh}}$ represents a microscale cohesive relation (traction-separation relation) that describes the microscale fracture at a point $\boldsymbol{x}$. Distinct microscale cohesive relations are used to characterize the fracture process inside the domain Ω (either matrix, fiber or matrix-fiber interface). In general, the cohesive relation depends on the local crack opening $\llbracket \boldsymbol{u} \rrbracket$ and possibly on internal variables $\boldsymbol{\kappa}$ and the orientation of the crack (for anisotropic cohesive relations), as given by the crack normal $\boldsymbol{m}$. The crack opening is given by

$$\llbracket \boldsymbol{u} \rrbracket = \boldsymbol{u}^{+} - \boldsymbol{u}^{-} \qquad \boldsymbol{x} \text{ on } \Gamma \tag{3}$$

with the superscripts + and - referring to the displacements on opposites sides of Γ. Observe that the periodic boundary conditions at points where the crack intersects the external boundary do not specify a crack opening as they relate displacements on essentially the same side of the crack surface. Indeed, subtracting the boundary conditions provides the following relation:

$$\begin{aligned} \llbracket \boldsymbol{u}(\boldsymbol{x}, t) \rrbracket &= \llbracket \boldsymbol{u}(\boldsymbol{x} + l_1 \boldsymbol{e}_1, t) \rrbracket \qquad \boldsymbol{x} \text{ on } \partial\Omega_3 \cap \Gamma \\ \llbracket \boldsymbol{u}(\boldsymbol{x}, t) \rrbracket &= \llbracket \boldsymbol{u}(\boldsymbol{x} + l_2 \boldsymbol{e}_2, t) \rrbracket \qquad \boldsymbol{x} \text{ on } \partial\Omega_4 \cap \Gamma \end{aligned} \tag{4}$$

hence the boundary conditions only indicate that the jump in displacements repeats itself periodically but otherwise do not specify the actual value of the jump. In the present formulation, the intention is to use classical cohesive elements at the microscale for which a separate nucleation criterion is not specified separately since it is implicitly given in the cohesive relation and depends only on the stress vector acting on the plane of the cohesive element. However, it is noted that an implementation based on XFEM would require a separate nucleation criterion that predicts the orientation of the microcrack typically based on the stress and/or the strain tensor.

3. Scale transition relations

3.1. Preliminaries

The Hill-Mandel condition, also known as the macrohomogeneity condition, refers to a scale transition requirement aimed at consistently preserving mechanical quantities appearing in the balance principles and constitutive relations at distinct scales. As indicated in [Hill, 1972], a natural

definition of a macrostress $\boldsymbol{\sigma}^{\mathrm{M}}$ and a macrostrain $\boldsymbol{\epsilon}^{\mathrm{M}}$ is based on volume averages of their microscale counterparts, i.e., averages of $\boldsymbol{\sigma}$ and $\boldsymbol{\epsilon}$. If the scale transition is based on an (unweighted) volume average, it was observed that, in general, the product of averages is different than the average of products, hence one has to guarantee consistency a priori. In particular, the Hill-Mandel condition most commonly used refers to the stress power at a macroscopic point, where it is required that $\boldsymbol{\sigma}^{\mathrm{M}} \cdot \dot{\boldsymbol{\epsilon}}^{\mathrm{M}} = \langle \boldsymbol{\sigma} \cdot \dot{\boldsymbol{\epsilon}} \rangle_{\Omega}$, where $\dot{\boldsymbol{\epsilon}}^{\mathrm{M}}$ is the time rate of change of the macrostrain, $\dot{\boldsymbol{\epsilon}}$ is the time rate of change of the microstrain and the notation $\langle \cdot \rangle_{\Omega} := (1/|\Omega|) \int_{\Omega} (\cdot) \mathrm{d}v$ refers to an average over an area per unit depth (for plane problems) or a volume (in three dimensions). The Hill-Mandel condition for the stress power needs to be extended in the present context to account for the rate of work associated to fracture.

The microscale information in a volume element Ω can be used to extract the macroscale behavior in the neighborhood of a point nominally located at a macroscopic crack. The volume element contains information pertaining to both the macroscopic cohesive traction-separation relation as well as a contribution from the surrounding bulk material. In order to extract the effective traction-separation relation, it is necessary to separate the response of the actual crack from the response of the surrounding bulk material. This is achieved by decomposing the kinematic and kinetic contributions associated to the bulk (i.e., $\Omega \setminus \Gamma$) and the crack (i.e., Γ) as indicated below.

3.2. Average bulk and fracture strains

Divide the domain Ω into complementary subdomains whose boundaries contain Γ and $\partial\Omega$, as shown schematically with dashed lines in Fig. 2. Inside these subdomains the displacement field is differentiable, hence the strain field is well-defined. Applying the divergence theorem in each subdomain and in view of (2), it follows that the volume average of the microscale strain tensor $\boldsymbol{\epsilon}$ is

$$\langle \boldsymbol{\epsilon} \rangle_{\Omega} := \frac{1}{|\Omega|} \int_{\Omega} \boldsymbol{\epsilon} \mathrm{d}v = \frac{1}{|\Omega|} \int_{\Omega} [\nabla \boldsymbol{u}]_{\mathrm{sym}} \, \mathrm{d}v = \frac{1}{|\Omega|} \int_{\partial\Omega} [\boldsymbol{u} \otimes \boldsymbol{n}]_{\mathrm{sym}} \, \mathrm{d}s - \frac{1}{|\Omega|} \int_{\Gamma} [[\![\boldsymbol{u}]\!] \otimes \boldsymbol{m}]_{\mathrm{sym}} \, \mathrm{d}s \tag{5}$$

where $\otimes$ is the tensor product, $[\boldsymbol{A}]_{\mathrm{sym}} := \frac{1}{2}\left(\boldsymbol{A} + \boldsymbol{A}^{\mathrm{T}}\right)$ refers to the symmetric part of a tensor $\boldsymbol{A}$, $[\![\boldsymbol{u}]\!]$ is the crack opening as defined in (3), $\boldsymbol{n}$ represents the outward normal unit vector to $\partial\Omega$ and $\boldsymbol{m}$ the normal unit vector pointing towards the + side of Γ (i.e., $\boldsymbol{m} = \boldsymbol{m}^{-} = -\boldsymbol{m}^{+}$, as indicated in Fig. 2). Line integrals in the subdomains are by convention performed in an anti-clockwise fashion, hence the + side needs to be interpreted according to the (local) parametrization of (segments) of Γ.

In the sequel, the periodic boundary conditions are used to identify a relation between different strain measures. The outward normal vectors on the sides $\partial\Omega_3$ and $\partial\Omega_4$ are, respectively, equal to the negative outward normal vectors on the sides $\partial\Omega_1$ and $\partial\Omega_2$ (see Fig. 2). Consequently, in view of (1), suppressing the time variable for simplicity, observing that $\boldsymbol{n} = \boldsymbol{n}_3 = -\boldsymbol{e}_1$ for points $\boldsymbol{x}$ on $\partial\Omega_3$ and using the fact that $|\Omega| = l_1 l_2$, it follows that

$$\begin{aligned} \frac{1}{|\Omega|} \int_{\partial\Omega_3} [\boldsymbol{u}(\boldsymbol{x}) \otimes \boldsymbol{n}]_{\mathrm{sym}} \, \mathrm{d}s &= \frac{1}{|\Omega|} \int_{\partial\Omega_3} [(\boldsymbol{u}(\boldsymbol{x} + l_1 \boldsymbol{e}_1) - l_1 \bar{\boldsymbol{\epsilon}} \boldsymbol{e}_1) \otimes \boldsymbol{n}_3]_{\mathrm{sym}} \, \mathrm{d}s \\ &= -\frac{1}{|\Omega|} \int_{\partial\Omega_3} [\boldsymbol{u}(\boldsymbol{x} + l_1 \boldsymbol{e}_1) \otimes \boldsymbol{e}_1]_{\mathrm{sym}} \, \mathrm{d}s + [\bar{\boldsymbol{\epsilon}} \boldsymbol{e}_1 \otimes \boldsymbol{e}_1]_{\mathrm{sym}} \ . \end{aligned} \tag{6}$$

For points $\boldsymbol{x}$ on $\partial\Omega_3$, the position vector $\boldsymbol{x} + l_1\boldsymbol{e}_1$ indicates a point on the opposite side, i.e., $\partial\Omega_1$ (see Fig. 2). Further, the outward normal unit vector $\boldsymbol{n}$ for points on $\partial\Omega_1$ is $\boldsymbol{n} = \boldsymbol{e}_1$. Consequently, the first integral on the right hand side of (6) can be alternatively expressed as an integral over $\partial\Omega_1$, i.e.,

$$-\frac{1}{|\Omega|}\int_{\partial\Omega_3}[\boldsymbol{u}(\boldsymbol{x}+l_1\boldsymbol{e}_1)\otimes\boldsymbol{e}_1]_{\text{sym}}\,\mathrm{d}s = -\frac{1}{|\Omega|}\int_{\partial\Omega_1}[\boldsymbol{u}(\boldsymbol{x})\otimes\boldsymbol{n}]_{\text{sym}}\,\mathrm{d}s$$

where $\boldsymbol{x}$ and $\boldsymbol{n}$ in the integral on the right hand side refer to, respectively, points on $\partial\Omega_1$ and the corresponding outward normal vector. Using the previous relation in (6) and suppressing the arguments gives

$$\frac{1}{|\Omega|}\int_{\partial\Omega_1}[\boldsymbol{u}\otimes\boldsymbol{n}]_{\text{sym}}\,\mathrm{d}s + \frac{1}{|\Omega|}\int_{\partial\Omega_3}[\boldsymbol{u}\otimes\boldsymbol{n}]_{\text{sym}}\,\mathrm{d}s = [\bar{\boldsymbol{\epsilon}}\boldsymbol{e}_1\otimes\boldsymbol{e}_1]_{\text{sym}}\ . \tag{7}$$

Using the same procedure in the $\boldsymbol{e}_2$ direction, it follows that

$$\frac{1}{|\Omega|}\int_{\partial\Omega_2}[\boldsymbol{u}\otimes\boldsymbol{n}]_{\text{sym}}\,\mathrm{d}s + \frac{1}{|\Omega|}\int_{\partial\Omega_4}[\boldsymbol{u}\otimes\boldsymbol{n}]_{\text{sym}}\,\mathrm{d}s = [\bar{\boldsymbol{\epsilon}}\boldsymbol{e}_2\otimes\boldsymbol{e}_2]_{\text{sym}}\ ,$$

which, in combination with (7), yields

$$\frac{1}{|\Omega|}\int_{\partial\Omega}[\boldsymbol{u}\otimes\boldsymbol{n}]_{\text{sym}}\,\mathrm{d}s = [\bar{\boldsymbol{\epsilon}}\boldsymbol{e}_1\otimes\boldsymbol{e}_1]_{\text{sym}} + [\bar{\boldsymbol{\epsilon}}\boldsymbol{e}_2\otimes\boldsymbol{e}_2]_{\text{sym}} = \bar{\boldsymbol{\epsilon}} \tag{8}$$

where the last identity follows from the (two-dimensional) identity tensor $\boldsymbol{I} = \boldsymbol{e}_1\otimes\boldsymbol{e}_1 + \boldsymbol{e}_2\otimes\boldsymbol{e}_2$ and the symmetry of $\bar{\boldsymbol{\epsilon}}$. A similar formula can be established for the three-dimensional case.

Using (8) in (5) provides a relation between the applied strain $\bar{\boldsymbol{\epsilon}}$, the average strain $\langle\boldsymbol{\epsilon}\rangle_\Omega$ in the bulk material and the average of the normal vector and the crack opening, namely

$$\bar{\boldsymbol{\epsilon}} = \langle\boldsymbol{\epsilon}\rangle_\Omega + \boldsymbol{\epsilon}^{\text{f}}\ , \tag{9}$$

where

$$\boldsymbol{\epsilon}^{\text{f}} := \frac{1}{|\Omega|}\int_\Gamma[[\![\boldsymbol{u}]\!]\otimes\boldsymbol{m}]_{\text{sym}}\,\mathrm{d}s\ . \tag{10}$$

Observe that, in contrast to the continuous case without cracks where $\bar{\boldsymbol{\epsilon}}$ and $\langle\boldsymbol{\epsilon}\rangle_\Omega$ coincide, these two quantities are different in the presence of a crack. In the context of a multiscale analysis, it is useful to interpret the result shown above as a kinematic decomposition of the "total" strain $\bar{\boldsymbol{\epsilon}}$ into a "bulk" strain $\langle\boldsymbol{\epsilon}\rangle_\Omega$ (strain in the uncracked material) plus an equivalent "fracture strain" $\boldsymbol{\epsilon}^{\text{f}}$, which is defined in (10). As shown in the sequel, the strains $\bar{\boldsymbol{\epsilon}}$, $\boldsymbol{\epsilon}^{\text{f}}$ and $\langle\boldsymbol{\epsilon}\rangle_\Omega$ will also represent, respectively, the applied strain, the fracture strain and the strain in the surrounding uncracked material of a periodic crack. However, depending on the method used to impose the applied strain, care needs to be exercised to properly interpret this quantity in order to prevent an artificial analysis with multiple parallel crack analysis as indicated in Appendix A.

3.3. Volume-averaged stress

Regarding the volume-averaged stress, making sequential use of the identity $\mathrm{div}\,(\boldsymbol{\sigma}\otimes\boldsymbol{x}) = \mathrm{div}\,\boldsymbol{\sigma}\otimes\boldsymbol{x} + \boldsymbol{\sigma}$, the equation of equilibrium, the divergence theorem, and the continuity of the traction acting on Γ, it follows that

$$\langle\boldsymbol{\sigma}\rangle_\Omega := \frac{1}{|\Omega|}\int_\Omega \boldsymbol{\sigma}\mathrm{d}v = \frac{1}{|\Omega|}\int_{\partial\Omega} \boldsymbol{t}\otimes\boldsymbol{x}\mathrm{d}s\,, \tag{11}$$

where $\boldsymbol{t} = \boldsymbol{\sigma}\boldsymbol{n}$ is the traction vector on the boundary $\partial\Omega$.

The expression (11) can be further specialized for anti-periodic traction boundary condition as

$$\langle\boldsymbol{\sigma}\rangle_\Omega = \sum_{i=1}^{2} \bar{\boldsymbol{t}}_i\otimes\boldsymbol{e}_i\,, \qquad \bar{\boldsymbol{t}}_i := \frac{1}{|\partial\Omega_i|}\int_{\partial\Omega_i}\boldsymbol{t}\mathrm{d}s \tag{12}$$

where $\bar{\boldsymbol{t}}_i, i = 1,2$ are the surface-averaged tractions on sides $\partial\Omega_i$ with $|\partial\Omega_1| = l_2$ and $|\partial\Omega_2| = l_1$. An equivalent formula applies for the three-dimensional case.

3.4. Rate of work relation and Hill-Mandel condition for volume element

The specific rate of external work P^{ext} done on the boundary of the volume element and the specific stress power P^{b} in the bulk material, both measured per unit area and per unit depth (in two dimensions) or per unit volume (in three dimensions) are defined, respectively, as

$$P^{\mathrm{ext}} := \frac{1}{|\Omega|}\int_{\partial\Omega}\boldsymbol{t}\cdot\dot{\boldsymbol{u}}\mathrm{d}s\,, \quad \text{and} \quad P^{\mathrm{b}} := \frac{1}{|\Omega|}\int_\Omega \boldsymbol{\sigma}\cdot\dot{\boldsymbol{\epsilon}}\mathrm{d}v\,.$$

The next step in the foregoing analysis is to relate these quantities to the rate of work of fracture (rate of work done by the traction on the crack surface Γ). To this end, consider again the subdomains indicated in Fig. 2. Recalling the identity

$$\mathrm{div}\left(\boldsymbol{\sigma}^{\mathrm{T}}\dot{\boldsymbol{u}}\right) = \mathrm{div}\boldsymbol{\sigma}\cdot\dot{\boldsymbol{u}} + \boldsymbol{\sigma}\cdot\nabla\dot{\boldsymbol{u}}\,,$$

which is applicable for points $\boldsymbol{x}\in\Omega\setminus\Gamma$ and further making use of the equilibrium equation (1), the strain-displacement relation (2) with $\nabla\dot{\boldsymbol{u}} = (\mathrm{d}/\mathrm{d}t)\nabla\boldsymbol{u}$ and the symmetry of $\boldsymbol{\sigma}$, it follows that the stress power can be expressed as

$$P^{\mathrm{b}} = \frac{1}{|\Omega|}\int_\Omega \mathrm{div}\left(\boldsymbol{\sigma}^{\mathrm{T}}\dot{\boldsymbol{u}}\right)\mathrm{d}v = \frac{1}{|\Omega|}\int_{\partial\Omega}\boldsymbol{t}\cdot\dot{\boldsymbol{u}}\mathrm{d}s - \frac{1}{|\Omega|}\int_\Gamma \boldsymbol{t}\cdot[\![\dot{\boldsymbol{u}}]\!]\mathrm{d}s\,,$$

where the last expression is obtained from the divergence theorem and Cauchy's theorem (i.e., $\boldsymbol{t} = \boldsymbol{\sigma}\boldsymbol{n}$ on $\partial\Omega$ and $\boldsymbol{t} = \boldsymbol{\sigma}\boldsymbol{m}$ on Γ). In the relation above, the traction on Γ refers to the traction acting on the Γ^- side, i.e., $\boldsymbol{t} = \boldsymbol{t}^- = \boldsymbol{\sigma}^-\boldsymbol{m}$ with $\boldsymbol{\sigma}^-$ referring to the stress tensor on the Γ^- side.

Combining the expressions for the external rate of work done on the volume element and the stress power it follows that

$$P^{\mathrm{ext}} = P^{\mathrm{b}} + P^{\mathrm{f}}\,, \tag{13}$$

where

$$P^{\mathrm{f}} := \frac{1}{|\Omega|}\int_{\Gamma} \boldsymbol{t}\cdot[\![\dot{\boldsymbol{u}}]\!]\mathrm{d}s \tag{14}$$

which indicates that the specific external power done on the volume element is equal to the specific stress power (on the bulk, uncracked material) plus the rate of work of fracture, which is defined in (14). Observe that, in accordance with the notational convention indicated above, Γ corresponds to the crack at a fully-failed state and hence it is not interpreted as a function of time. During the overall cracking process, at a given time t, some segments in Γ may be fully-separated, some may be partially cracked and others may be still uncracked. Prior to cracking, uncracked segments do not contribute to the integral in (14) since the displacement is continuous in an undamaged segment.

In accordance with a classical multiscale approach, the macroscopic bulk stress and bulk strain are taken as the volume average of their microscopic counterparts. In view of the kinematical decomposition (9) and in line with the approach indicated above for the effective bulk stress and strain, the effective equivalent strain associated with a macroscopic cohesive surface is identified as $\boldsymbol{\epsilon}^{\mathrm{f}}$ as defined in (10).

The version of Hill-Mandel's requirement for the whole volume element (i.e., bulk and cracked parts), can be expressed in terms of surface data, i.e.,

$$\langle\boldsymbol{\sigma}\rangle_{\Omega}\cdot\dot{\bar{\boldsymbol{\epsilon}}} = P^{\mathrm{ext}} = \frac{1}{|\Omega|}\int_{\partial\Omega}\boldsymbol{t}\cdot\dot{\boldsymbol{u}}\mathrm{d}s\,. \tag{15}$$

For periodic boundary conditions, using an approach similar as the one used in the previous subsections, it can be shown that the specific external power done on the volume element is such that

$$\frac{1}{|\Omega|}\int_{\partial\Omega}\boldsymbol{t}\cdot\dot{\boldsymbol{u}}\mathrm{d}s = \bar{\boldsymbol{t}}_1\cdot\dot{\bar{\boldsymbol{\epsilon}}}\boldsymbol{e}_1 + \bar{\boldsymbol{t}}_2\cdot\dot{\bar{\boldsymbol{\epsilon}}}\boldsymbol{e}_2 = \langle\boldsymbol{\sigma}\rangle_{\Omega}\cdot\dot{\bar{\boldsymbol{\epsilon}}}\,,$$

where the surface-averaged tractions $\bar{\boldsymbol{t}}_1$ and $\bar{\boldsymbol{t}}_2$ and the last relation follows from (12). The previous analysis confirms that periodic boundary conditions are sufficient to satisfy the "global" Hill-Mandel condition (i.e., bulk and crack combined). However, for the purpose of the present analysis, a more relevant statement is a separate scale transition relation for the crack. This analysis is presented in Sec. 4.1. To this end, some details on the notion of a periodic crack are provided in Appendix A.

4. Equivalent macroscopic crack

4.1. Equivalent macroscopic crack length

The microscopic crack Γ (or, the equivalent crack surface Γ^{s} see Appendix A), can be represented at the macroscopic level by an equivalent macroscopic straight (differential) crack segment denoted as Γ^{f} and characterized geometrically by its orientation given by a unit normal vector $\boldsymbol{m}^{\mathrm{f}}$ and a nominal length $\left|\Gamma^{\mathrm{f}}\right|$ (per unit depth for plane problems) or a nominal area (for three-dimensional problems), as illustrated in Fig. 3. The path of a crack at the microscale is typically affected by the microstructure of the composite material both in terms of geometrical features (e.g.,

distribution of fibers, fiber diameters, volume fractions) as well as the fracture properties of the constituents, interfaces and the presence of flaws (Ponnusami et al., 2015). The microscale volume element should reproduce these features to assure convergence in a multiscale sense. More generally, geometrical features at each length scale are resolved with a characteristic accuracy, i.e., what appears as a complex crack pattern at the lower length scale within a volume element is typically resolved "locally" as a straight crack (differential) segment at the larger scale. The orientation of a nominally straight macroscopic crack segment is given by a unit normal vector $\boldsymbol{m}^{\mathrm{f}}$ that can be defined based on the fully-failed state as

$$\boldsymbol{m}^{\mathrm{f}} := \langle \boldsymbol{m} \rangle_{\Gamma} \ , \tag{16}$$

where the notation $\langle \cdot \rangle_{\Gamma} := (1/|\Gamma|) \int_{\Gamma} (\cdot) \mathrm{d}s$, representing crack-averaged quantities, is introduced for convenience. This average contains contributions from all crack segments of Γ, including bifurcations and disconnected parts. In principle the vector $\boldsymbol{m}^{\mathrm{f}}$ could evolve during the loading process but, to simplify the procedure, it is assumed to be independent of time and obtained through post-processing of the fully-failed state. Care must be taken to compute separate contributions independently of the choice of the positive and negative sides of segments in Γ (Westbroek, 2017).

On the other hand, a straight macroscopic crack segment of nominal length $\left|\Gamma^{\mathrm{f}}\right|$ should represent the accumulated effect of microcracks. As opposed to quantities defined per unit volume, a definition of the equivalent (or effective) unit macroscopic crack length per unit depth (or per unit area in a fully three-dimensional framework) and its relation with the microscale crack length (or area) is relevant since the macroscopic work of fracture per unit macroscopic length (or area) should coincide with the overall work of fracture in a microscopic volume element.

Several options are available for the purpose of identifying $\left|\Gamma^{\mathrm{f}}\right|$, which should relate the microscale crack length $|\Gamma|$ to a macroscopic differential element. One option is to determine the shifting mapping given in (A.1), construct the equivalent crack domain Ω^{s} and project it onto a line perpendicular to a given nominal crack normal vector $\boldsymbol{m}^{\mathrm{f}}$ to compute a characteristic length $\left|\Gamma^{\mathrm{f}}\right|$ (see illustration in Fig.3). A second option, which is adopted here for simplicity since it avoids determining the shifting mapping, is to propose a nominal length (or area in three dimensions) computed as follows: Let

$$\left|\Gamma^{\mathrm{f}}_{\mathrm{min}}\right| := \min\left(\frac{l_1}{\left|\boldsymbol{n}_2 \cdot \boldsymbol{m}^{\mathrm{f}}\right|}, \frac{l_2}{\left|\boldsymbol{n}_1 \cdot \boldsymbol{m}^{\mathrm{f}}\right|} \right) \qquad \left|\Gamma^{\mathrm{f}}_{\mathrm{max}}\right| := \max\left(\frac{l_1}{\left|\boldsymbol{n}_2 \cdot \boldsymbol{m}^{\mathrm{f}}\right|}, \frac{l_2}{\left|\boldsymbol{n}_1 \cdot \boldsymbol{m}^{\mathrm{f}}\right|} \right) \qquad r := \frac{\left|\Gamma^{\mathrm{f}}_{\mathrm{max}}\right|}{\left|\Gamma^{\mathrm{f}}_{\mathrm{min}}\right|} \ , \tag{17}$$

and define the macroscopic crack length as

$$\left|\Gamma^{\mathrm{f}}\right| := \begin{cases} \left|\Gamma^{\mathrm{f}}_{\mathrm{min}}\right| & \text{if } r \geq r_{\mathrm{max}} \ , \\ \\ \left|\Gamma^{\mathrm{f}}_{\mathrm{max}}\right| & \text{if } r < r_{\mathrm{max}} \ . \end{cases} \tag{18}$$

In the definition given above, the length of the equivalent crack Γ^{f} is estimated based on the orientation of the macroscopic crack (given by $\boldsymbol{m}^{\mathrm{f}}$), the approximate number of crossings through the volume element Ω (given by r) and the dimensions l_1 and l_2 of Ω (as indicated in Fig. 2). Due to periodicity, if $\boldsymbol{m}^{\mathrm{f}}$ is neither vertical nor horizontal, an equivalent crack can be nominally

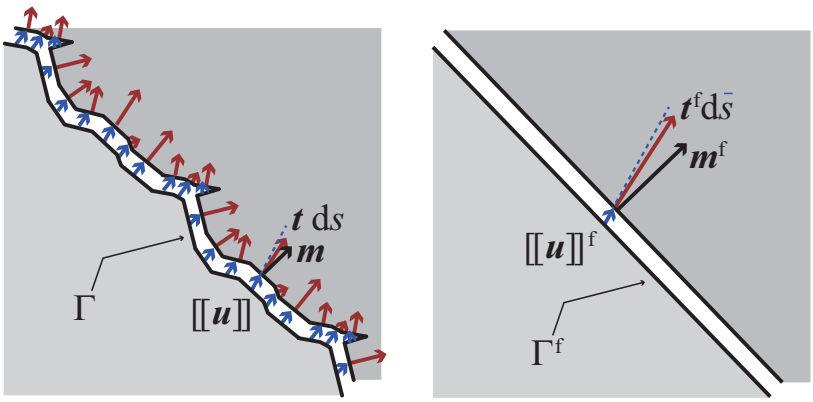

Figure 3: Illustration of the Hill-Mandel requirement for an equivalent macrocrack Γ^{f}: the average of the rate of work done by the local traction on the local crack opening rate has to match the rate of work done by the equivalent traction on the equivalent crack opening rate. Observe that the equivalent macroscopic traction acts on a macroscopic differential $\mathrm{d}\bar{s}$ representing length per unit depth (for plane problems) or area (for three-dimensional problems).

interpreted as a collection of inclined straight segments of length $\left|\Gamma^{\mathrm{f}}_{\mathrm{min}}\right|$ (top/bottom or left/right) in Ω plus a partial segment from a horizontal to a vertical side (albeit at a different angle than the other inclined segments, but with approximately the same length). In that case, the total length is expressed as $r\left|\Gamma^{\mathrm{f}}_{\mathrm{min}}\right| = \left|\Gamma^{\mathrm{f}}_{\mathrm{max}}\right|$. A horizontal (or near-horizontal) crack with $\boldsymbol{m}^{\mathrm{f}} \approx \boldsymbol{n}_2$ corresponds to an infinite (or very large) number of crossings for which r is greater than the cut-off value r_{max} and therefore has a nominal length l_1. Similarly, a vertical (or near-vertical) crack $\boldsymbol{m}^{\mathrm{f}} \approx \boldsymbol{n}_1$ has a nominal length l_2.

4.2. Crack-based Hill-Mandel condition

In Sec. 3.4 it was indicated that in order to study the macroscale behavior of a crack, a version of the Hill-Mandel condition is required for the crack itself (as opposed to the volume element surrounding the crack). To this end, it is observed that, from (13), (15) and (9), the specific external power done on the volume element can alternatively be written as

$$\langle\boldsymbol{\sigma}\rangle_\Omega \cdot \dot{\bar{\boldsymbol{\epsilon}}} = \langle\boldsymbol{\sigma}\rangle_\Omega \cdot \langle\dot{\boldsymbol{\epsilon}}\rangle_\Omega + \langle\boldsymbol{\sigma}\rangle_\Omega \cdot \dot{\boldsymbol{\epsilon}}^{\mathrm{f}} = \frac{1}{|\Omega|}\int_\Omega \boldsymbol{\sigma}\cdot\dot{\boldsymbol{\epsilon}}\mathrm{d}v + \frac{1}{|\Omega|}\int_\Gamma \boldsymbol{t}\cdot[\![\dot{\boldsymbol{u}}]\!]\mathrm{d}s\,.$$

Consequently, the Hill-Mandel condition for the crack is taken as

$$\langle\boldsymbol{\sigma}\rangle_\Omega \cdot \dot{\boldsymbol{\epsilon}}^{\mathrm{f}} = P^{\mathrm{f}} = \frac{1}{|\Omega|}\int_\Gamma \boldsymbol{t}\cdot[\![\dot{\boldsymbol{u}}]\!]\mathrm{d}s\,, \tag{19}$$

which, if satisfied, would immediately imply from the "global" Hill-Mandel condition that the Hill-Mandel condition for the bulk, uncracked material (i.e., $\langle\boldsymbol{\sigma}\rangle_\Omega \cdot \langle\dot{\boldsymbol{\epsilon}}\rangle_\Omega = P^{\mathrm{b}}$) is also satisfied. In view of (10), relation (19) can be further expressed as

$$\frac{1}{|\Gamma|}\int_\Gamma \langle\boldsymbol{\sigma}\rangle_\Omega \cdot [[\dot{\boldsymbol{u}}]]\otimes\boldsymbol{m}]_{\mathrm{sym}}\,\mathrm{d}s = \frac{1}{|\Gamma|}\int_\Gamma \boldsymbol{\sigma}\cdot[[\dot{\boldsymbol{u}}]]\otimes\boldsymbol{m}]_{\mathrm{sym}}\,\mathrm{d}s\,, \tag{20}$$

where it is noted that for convenience, but without loss of generality, both sides of (19) have been multiplied by a constant term $|\Omega|/|\Gamma|$. This scaling is useful since it eliminates the length-to-volume ratio that otherwise may obscure the existence of a representative volume element when comparing volume elements of different sizes.

From (20) the macrohomogeneity condition for the crack can be expressed as

$$\left\langle (\langle \boldsymbol{\sigma} \rangle_\Omega \, \boldsymbol{m} - \boldsymbol{t}) \cdot [\![\dot{\boldsymbol{u}}]\!] \right\rangle_\Gamma = 0 \, . \tag{21}$$

Relation (21) indicates that the volume-averaged stress $\langle \boldsymbol{\sigma} \rangle_\Omega$, acting on the local crack normal $\boldsymbol{m}$ and working on the crack opening rate $[\![\dot{\boldsymbol{u}}]\!]$, has to represent on average the working of the local crack surface traction $\boldsymbol{t} = \boldsymbol{\sigma} \boldsymbol{m}$ on the crack opening rate. In contrast with the global Hill-Mandel conditions, the crack-based Hill-Mandel condition cannot be satisfied a priori through the boundary conditions. Instead, the approach adopted here is to (approximately) enforce the macro-homogeneity condition *a posteriori* in terms of the effective fields. Up to this point the macroscopic fields associated with the fracture process have not been defined, except for the fracture strain given in (10), the crack orientation given in (16) and the nominal crack length given in (18). An effective macroscopic crack opening rate, denoted as $[\![\dot{\boldsymbol{u}}]\!]^{\mathrm{f}}$, can be defined as

$$[\![\dot{\boldsymbol{u}}]\!]^{\mathrm{f}} := \frac{|\Gamma|}{\left|\Gamma^{\mathrm{f}}\right|} \langle [\![\dot{\boldsymbol{u}}]\!] \rangle_\Gamma \, . \tag{22}$$

The effective crack opening rate $[\![\dot{\boldsymbol{u}}]\!]^{\mathrm{f}}$ can be computed incrementally and in general varies throughout the loading process even if the externally applied rate $\dot{\bar{\boldsymbol{\epsilon}}}$ is constant.

In terms of kinetics, denote by $\boldsymbol{t}^{\mathrm{f}}$ an as yet to be defined effective macroscopic traction acting on the macrocrack surface. Using effective quantities, the Hill-Mandel condition (20) (or (21)) for the crack can be divided into two separate requirements, which are assumed to be approximately satisfied, namely

$$\begin{aligned} \left|\Gamma^{\mathrm{f}}\right| \, \boldsymbol{t}^{\mathrm{f}} \cdot [\![\dot{\boldsymbol{u}}]\!]^{\mathrm{f}} &\approx |\Gamma| \left\langle \boldsymbol{t} \cdot [\![\dot{\boldsymbol{u}}]\!] \right\rangle_\Gamma \qquad \text{and} \\ \left|\Gamma^{\mathrm{f}}\right| \, \boldsymbol{t}^{\mathrm{f}} \cdot [\![\dot{\boldsymbol{u}}]\!]^{\mathrm{f}} &\approx |\Gamma| \left\langle \langle \boldsymbol{\sigma} \rangle_\Omega \, \boldsymbol{m} \cdot [\![\dot{\boldsymbol{u}}]\!] \right\rangle_\Gamma \, . \end{aligned} \tag{23}$$

The first expression in (23) refers to a scale transition based purely on quantities on the crack surface while the second condition consistently couples this quantity with relevant information associated to the surrounding volume element through the volume-averaged stress tensor $\langle \boldsymbol{\sigma} \rangle_\Omega$. In general, these two requirements may not be satisfied simultaneously as the crack-averaged traction may differ from the volume-averaged stress acting on the local crack normal, although these two quantities would coincide through a limit process if the computational domain Ω becomes essentially the crack surface Γ itself.

One approach to satisfy the requirements indicated in (23) is to *define* the effective traction $\boldsymbol{t}^f$ directly from the crack-based Hill-Mandel condition, which automatically guarantees that the macrohomogenity condition is satisfied. An alternative approach, as adopted in the present work, is to propose an expression for the effective traction that contains one (or more) model parameters used to enforce the scale transition conditions. The requirements indicated in (23) motivate the following definition for the effective traction on the equivalent macroscopic crack:

$$\boldsymbol{t}^{\mathrm{f}} := \alpha \boldsymbol{t}^{\mathrm{f}}_\Gamma + (1 - \alpha) \boldsymbol{t}^{\mathrm{f}}_\Omega \, , \tag{24}$$

where α is a weighting factor and

$$\boldsymbol{t}^{\mathrm{f}}_{\Gamma} := \langle \boldsymbol{t} \rangle_{\Gamma} \qquad \boldsymbol{t}^{\mathrm{f}}_{\Omega} := \langle \boldsymbol{\sigma} \rangle_{\Omega} \, \boldsymbol{m}^{\mathrm{f}} \, . \tag{25}$$

The weighting factor α is introduced as a model parameter to enforce scale transition conditions, as explained in the sequel, with the case $\alpha = 1$ corresponding to an effective traction based only on a crack-averaged traction $\boldsymbol{t}^{\mathrm{f}}_{\Gamma}$ and the case $\alpha = 0$ representing an effective traction based only on a traction $\boldsymbol{t}^{\mathrm{f}}_{\Omega}$, which is a volume-averaged stress tensor acting on the nominal unit normal vector.

From a different perspective, the proposed form for the effective traction given in (24) implies that at a larger length scale, the effective cohesive relation may be coupled to elastic and/or inelastic phenomena occurring in the vicinity of the crack and may not be fully uncoupled (e.g., plastic deformations in the material surrounding the crack are accounted for in the cohesive relation through the stress averaged in the vicinity of a crack).

In order to monitor during a simulation the enforcement of the crack-based Hill-Mandel condition and in view of (23) and (22), it is convenient to define two residuals as follows:

$$R_{\Gamma} := \left| |\Gamma^{\mathrm{f}}| \, \boldsymbol{t}^{\mathrm{f}} \cdot [\![\dot{\boldsymbol{u}}]\!]^{\mathrm{f}} - |\Gamma| \left\langle \boldsymbol{t} \cdot [\![\dot{\boldsymbol{u}}]\!] \right\rangle_{\Gamma} \right| \qquad \text{and} \qquad R_{\Omega} := \left| |\Gamma^{\mathrm{f}}| \, \boldsymbol{t}^{\mathrm{f}} \cdot [\![\dot{\boldsymbol{u}}]\!]^{\mathrm{f}} - |\Gamma| \left\langle \langle \boldsymbol{\sigma} \rangle_{\Omega} \, \boldsymbol{m} \cdot [\![\dot{\boldsymbol{u}}]\!] \right\rangle_{\Gamma} \right| \, . \tag{26}$$

The residuals R_{Γ} and R_{Ω}, which generally depend on time, can be used to monitor the deviation between the computed rate of work on the crack itself and the homogenized rate of work both in terms of local homogeneity on the crack surface (through R_{Γ}) as well as in terms of consistent coupling with the surrounding bulk material (through R_{Ω}). Ideally both R_{Γ} and R_{Ω} should be sufficiently small for a converged solution.

The definition of the macroscopic quantities adopted here is seen as a computationally convenient one, but other options may also be possible. However, the relevant issues are that (i) the balance of energy needs to be preserved quantitatively across scales and (ii) the macroscopic quantities should conform to a continuum formulation that does not (explicitly) take the microstructure into account.

4.3. Macrocrack nucleation criterion and effective traction-separation relation for a composite

An effective constitutive model that can be used at the macroscopic scale to describe the onset and evolution of a macrocrack consists of an initiation (nucleation) criterion and a traction-separation relation. This type of model is intended for numerical simulations of fracture using, for example, the XFEM framework. In this context, the initiation criterion requires a critical value of a stress and/or strain-based measure to detect the onset of failure together with an orientation of the crack. After identification of the orientation of the macrocrack, the crack propagation can be determined based on a (rate-independent) effective traction-separation can be obtained for an equivalent crack in the general form

$$\boldsymbol{t}^{\mathrm{f}} = \boldsymbol{f}^{\mathrm{f}}_{\mathrm{coh}} \left([\![\boldsymbol{u}]\!]^{\mathrm{f}}, \boldsymbol{\kappa}^{\mathrm{f}}, \boldsymbol{m}^{\mathrm{f}} \right) \tag{27}$$

where the vector-valued function $\boldsymbol{f}^{\mathrm{f}}_{\mathrm{coh}}$ represents the (macroscale) cohesive relation that describes the net effect of fracture in the neighborhood of a macroscopic point. The traction-separation

relation can be obtained as a function of the macroscopic crack opening through time-integration of the macroscopic crack opening rate. In addition, a (possibly anisotropic) mixed-mode behavior can be indicated as a function of the effective crack normal $\boldsymbol{m}^{\mathrm{f}}$ (generally with respect to configuration-dependent axes that describe the anisotropy). For the present purposes, a (transversely) isotropic configuration is assumed, hence only an explicit dependence on the crack normal is indicated. Effective loading and unloading conditions can be captured with a set of internal variables $\boldsymbol{\kappa}^{\mathrm{f}}$. In general one may choose a convenient phenomenological traction-separation relation based on considerations of efficiency and accuracy, i.e., a simple relation, preferably one that is readily available in existing implementations, which can nevertheless accurately condense the results of the multiscale simulations. Moreover, the effective (macroscopic) traction-separation relation may be, in general, different than the relations used at the microscopic level (e.g., fracture mechanisms and material symmetries are expected to be different at distinct length scales).

In a classical formulation of a traction-separation relation, the orientation of the crack is assumed to be known a-priori (e.g., a "weak" interface between two materials), and the initiation criterion is taken care of by the value of the fracture strength. However, in the general case, the crack orientation is not known a-priori hence the traction-separation relation needs to be complemented with an effective nucleation criterion that predicts the orientation of the crack surface based on the applied strain and/or the corresponding applied stress prior to fracture. This relation, which forms part of the constitutive model, can be formally written as

$$\boldsymbol{m}^{\mathrm{f}} = \boldsymbol{m}_{\mathrm{coh}}\left(\langle\boldsymbol{\sigma}\rangle_{\Omega}\,,\,\overline{\boldsymbol{\epsilon}}\right) \tag{28}$$

where $\boldsymbol{m}_{\mathrm{coh}}$ is a function that depends on the state of stress prior to cracking as measured by the volume-averaged stress tensor $\langle\boldsymbol{\sigma}\rangle_{\Omega}$ and/or the applied strain $\overline{\boldsymbol{\epsilon}}$. In this formulation the nucleation criterion is partly given by the fracture strength in (27) and partly given by a relation of the type shown in (28) (see, e.g., (Hille et al., 2009)).

The proposed methodology is to calibrate an effective traction-separation relation by conducting a parametric study with representative macroscopic loading conditions, typically under proportional loading that represents a given mixed-mode ratio. In this fashion, the so-called FE^2 approach is replaced by a set of pre-determined effective responses. The effective traction-separation relation can be used in a macroscale simulation if the macroscopic loading matches the calibrated mixed-mode loading state. Proportional unloading and re-loading can be accounted for by effective history variables of the model. For non-proportional loading conditions, this approach may not provide the proper path-dependent response, but in many cases of practical interest it can provide a reasonable approximation as long as the deviation from proportional loading remains small. The next section deal with the numerical implementation and illustration of the general methodology.

4.4. Numerical implementation

The method chosen to numerically solve the microscale problem (1) is to embed cohesive elements along the edges of *all* bulk elements used to discretize the composite material that occupies the region Ω. An alternative approach is to use the extended finite element method, however the cohesive element route provides a simple and robust method in order to impose the periodicity conditions at crossing points. Furthermore, an embedded cohesive element approach typically can

account for crack bifurcations in a relatively straightforward fashion, whereas this is somewhat more difficult using (current) versions of the XFEM framework. The microscale problem was solved numerically with the finite element package Abaqus using an implicit scheme. For simplicity, mode-independent, bilinear traction-separation relations are used to describe the fracture process in the cohesive elements at the microscale. The term bilinear in this context refers to a linear "elastic" loading part followed by a linear softening regime.

Material periodicity is assumed at the microstructural level in the computational domain Ω, although the secondary phase (i.e., fibers) is randomly distributed. An unstructured mesh with triangular elements is used.

In a typical simulation, the elastic properties of the phases are given as well as the fracture properties of the phases and the interface between them. In the case of a cross-section perpendicular to the fiber direction in an unidirectional fiber-reinforced composite, the fiber volume fraction and the fiber diameter is given and a random distribution of fibers is assumed. Details of representative simulations for the microscale problem (1) are given in subsequent sections. An important step once a problem has been solved for a given strain (up to complete failure), is to extract the average response of the volume element (post-processing).

For post-processing purposes, it is assumed that a typical microscopic volume element is subjected to a proportional loading of the type $\overline{\boldsymbol{\epsilon}}(t) = c(t)\boldsymbol{\epsilon}_0$ from $t = 0$ to a final time $t = t_F$, at which point the volume element is considered to have failed (i.e., the effective traction is zero). The scalar-valued function $c(t)$ scales the (constant) strain tensor $\boldsymbol{\epsilon}_0$ and may be taken as a linear function for a nominally constant strain rate, i.e., $c(t) = t/t_F$.

After the geometrical characteristics of the macroscopic crack have been established, the time history of the crack nucleation and growth can be postprocessed from $t = 0$ to $t = t_F$ to determine the effective traction-separation relation.

A mesh refinement analysis indicates that the effective fracture response converges (details can be found in Westbroek (2017)). The generation of effective traction-separation relations can be carried out for a large number of combinations of model and geometrical parameters. The result of this process is a material database that can be used to create a correlation between material properties, configurations and load cases. This may be achieved through a systematic algorithm but lies outside of the scope of the present work. An application of this procedure for fiber-reinforced composites can be found in (van Hoorn, 2016), albeit using a different post-processing procedure. In the present work, a selected number of examples are shown in the subsequent sections to illustrate the process of generating the data.

5. Verification of scale transition relations.

The first step to verify the computational framework is to study whether the scale transition approach yields the anticipated results in terms of the crack-averaged Hill-Mandel condition. It is noted that this section pertains to scale transition relations, while the issue of establishing a *representative* volume element is dealt with in the Sec. 6.

5.1. Simulation setup and material parameters

The scale transition relation is analyzed in this section using a typical microscopic volume element consisting of a $75\mu\text{m} \times 75\mu\text{m}$ cross-section perpendicular to the fiber direction. The fibers

Table 1: Mechanical properties of the reference material.

Phase	Parameter	Symbol	Value	Units
Matrix	Young's modulus	$E^{(m)}$	3.5	GPa
	Poisson's ratio	$\nu^{(m)}$	0.35	[-]
	Fracture strength	$\sigma_{\mathrm{c}}^{(m)}$	50	MPa
	Fracture energy	$G_{\mathrm{c}}^{(m)}$	0.05	N/mm (= kJ/m^2)
Fiber	Young's modulus	$E^{(f)}$	19 (transverse)	GPa
	Poisson's ratio	$\nu^{(f)}$	0.23	[-]
	Fracture strength	$\sigma_{\mathrm{c}}^{(f)}$	100	MPa
	Fracture energy	$G_{\mathrm{c}}^{(f)}$	0.1	N/mm (= kJ/m^2)
Fiber-matrix interface	Fracture strength	$\sigma_{\mathrm{c}}^{(i)}$	25	MPa
	Fracture energy	$G_{\mathrm{c}}^{(i)}$	0.025	N/mm (= kJ/m^2)

have a diameter of 10μm and the volume element has a fiber volume fraction close to 50%. The volume element is subjected to a laterally-constrained uniaxial extension with periodic boundary conditions. The applied strain is proportional to $\boldsymbol{\epsilon}_0 = \epsilon_0 \boldsymbol{e}_1 \otimes \boldsymbol{e}_1$ and is henceforth referred to as load case 1.

Bilinear, mode-independent traction-separation relations, as described in Sec. 4.4, are used for the matrix and the fibers as well as the interfaces between them. The material properties used in the simulations are given in Table 1, namely the elastic properties (Young's modulus E and Poisson's ratio ν), the equivalent fracture strength σ_{c} and the equivalent fracture energy G_{c}. The elastic properties correspond to a representative fiber/epoxy combination, namely IM7 fibers and 5230-1 epoxy, with the relevant elastic stiffness of the fibers being the transverse modulus (note that this value is typically significantly lower than the stiffness in the fiber direction). Fracture properties were not readily available for these specific materials but representative values for fiber/matrix composites were taken from (Alfaro et al., 2010b). The fracture properties for the interface (sizing) are chosen to represent a relatively weak interface. The value of the fracture strength of the fibers loaded in the transverse direction is difficult to obtain, but, as shown below, no fiber cracking was observed in the simulations in accordance with experimental results for laterally loaded, single-ply unidirectional composites (Hobbiebrunken et al., 2006).

The cohesive stiffness chosen for all cohesive relations is $K = 10^8$ N/mm^3. For some simulations, a viscous regularization (as implemented in Abaqus) was used to achieve a convergent result (in terms of equilibrium in a quasi-static loading) with a viscous parameter of 10^{-4}MPa $\cdot$ s^{-1}.

5.2. Verification of crack-based Hill-Mandel condition

The fully-failed state of the microscopic volume element under laterally-constrained axial extension (load case 1) is shown in Fig. 4, where a mostly vertical periodic crack appears. Due to the relatively weak interface between the fibers and the matrix (see Table 1), it can be observed that the crack preferentially propagates along the fiber-matrix interfaces, bridging through the matrix

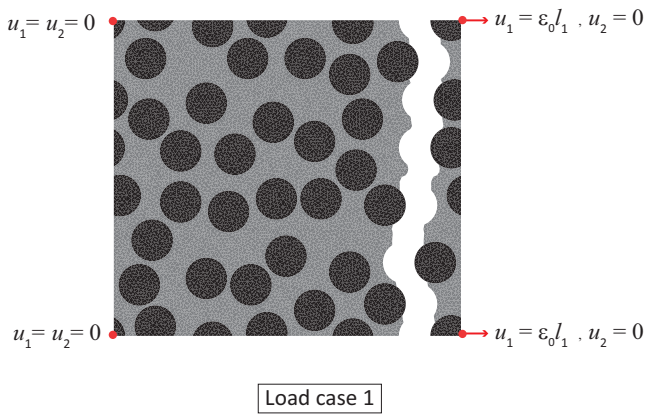

Figure 4: Fully-failed volume element under periodic boundary conditions representing a laterally-constrained extension.

between adjacent interfaces. This crack pattern is typically observed in laterally-loaded unidirectional composites (Hobbiebrunken et al., 2006).

The time-history of various power measures are shown in Fig. 5 as functions of a time-like process parameter (normalized by the final time of the simulation, t_F). The solid lines in the figure represent averages of products (either traction times crack opening rates or stress times strain rates), averaged either in the bulk, crack or external boundary and expressed per unit volume (in this case per unit area and per unit depth for plane strain simulations). The dashed lines represent products of effective or averaged quantities as indicated in the legend (i.e., either effective or averaged tractions times effective crack opening rates or averaged stress times averaged strain rates). The figure also includes a so-called cohesive "bulk" power, denoted as P^* in the figure, associated to cohesive elements that do not contribute to the crack but nevertheless experience a non-zero opening. This term does not appear in the theory developed in Sec. 3 and Sec. 4 since it is a characteristic of the numerical method used and not of the continuum theory. As may be observed in the figure, a portion of the elastic strain energy is stored due to an "elastic" opening of the cohesive elements. The stored (elastic) energy in these cohesive elements is not dissipated and, in the context of balance of power, it may be combined with the strain energy measured in the bulk elements. It is noted that these cohesive elements affect the elastic response, hence the MVE response should not directly be used to predict the elastic properties of the composite. However, their effect on the fracture properties is negligible.

As may be inferred from Fig. 5, the externally-applied power on the microscopic volume element is initially stored as elastic strain energy in the bulk and in the "elastic" response of the cohesive elements. As the applied deformation increases, microcracks initiate at various locations in the MVE, propagate and coalesce, forming a periodic (macroscopic) crack. The load-bearing capacity of the MVE decreases as the externally-applied displacement increases until it can no longer transmit forces and it is fully-failed. As shown in Fig. 5, the "global" Hill-Mandel condi-

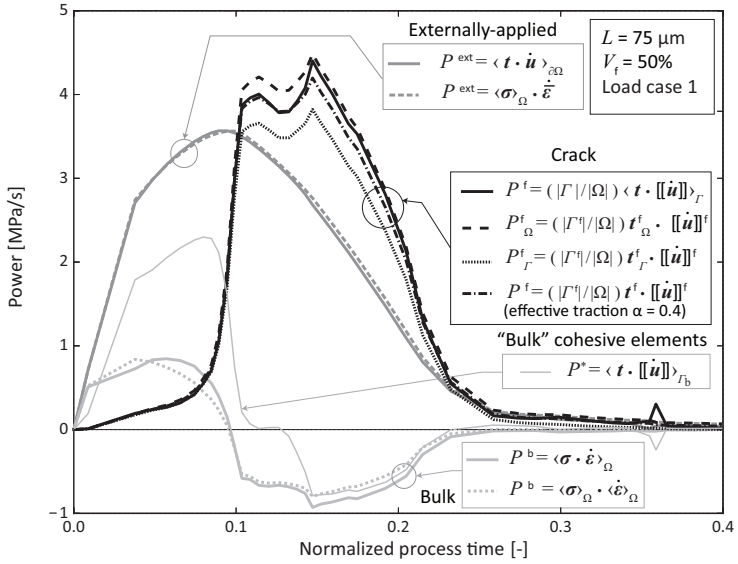

Figure 5: Crack and volume-averaged measures of the applied power P^{ext}, the power in the bulk P^b and various measures of the power in the crack P^{f} as a function of a time-like process parameter for a $75\mu\text{m} \times 75\mu\text{m}$ microscopic volume element under laterally-constrained axial extension (load case 1). The solid lines are averages of products and the dashed lines are products of averages and/or effective quantities.

tion given in (15) is satisfied, to within numerical accuracy, since periodic boundary conditions have been enforced. More relevant for the present discussion is the crack-based Hill-Mandel condition that requires special attention. As shown in the figure, using the crack-averaged traction $\boldsymbol{t}^{\text{f}}_{\Gamma}$ and the volume-averaged traction $\boldsymbol{t}^{\text{f}}_{\Omega}$ from (25) together with the effective crack opening rate $[\![\dot{\boldsymbol{u}}]\!]^{\text{f}}$ and the nominal (macroscopic) crack length $\left|\Gamma^{\text{f}}\right|$ from (17)-(18) (see Sec.4.4) provide, respectively, upper and lower approximations to the actual energy dissipation rate $|\Gamma| \left\langle \boldsymbol{t} \cdot [\![\dot{\boldsymbol{u}}]\!] \right\rangle_{\Gamma}$ due to the cracking process. With the choice of the value $\alpha = 0.4$ in this example, the effective traction on the equivalent macroscopic crack $\boldsymbol{t}^{\text{f}}$ as given in (24) and acting on the equivalent macroscopic crack provides an improved matching for the crack-based Hill-Mandel condition (see Fig. 5). In terms of a traction-separation relation, Fig. 6 shows the effective response of the microscopic volume element based on three values of the parameter α, namely $\alpha = 0, 0.4, 1$. The results are reported in terms of the normal components of the traction and the crack opening displacement, which are computed as

$$t^{\text{f}}_{\text{n}} := \boldsymbol{t}^{\text{f}} \cdot \boldsymbol{m}^{\text{f}} \qquad [\![u]\!]^{\text{f}}_{\text{n}} := [\![\boldsymbol{u}]\!]^{\text{f}} \cdot \boldsymbol{m}^{\text{f}} \, .$$

The tangential component was found to be negligible for this loading case. The optimal value of the weighting factor in this example, $\alpha = 0.4$, was found based on a direct parametric search (best approximation). In principle the procedure to find the optimal value can be carried out automatically, but a direct approach was deemed sufficient for the present purposes.

Further testing for other loading cases and MVEs, not shown here for reasons of conciseness, indicates that the optimal values of α can vary between 0 and 1 depending on the size of the MVE and its loading. In some cases, distinct optimal values are required for distinct realizations of nominally the same microstructure under the same loading. It is relevant to indicate that, based on

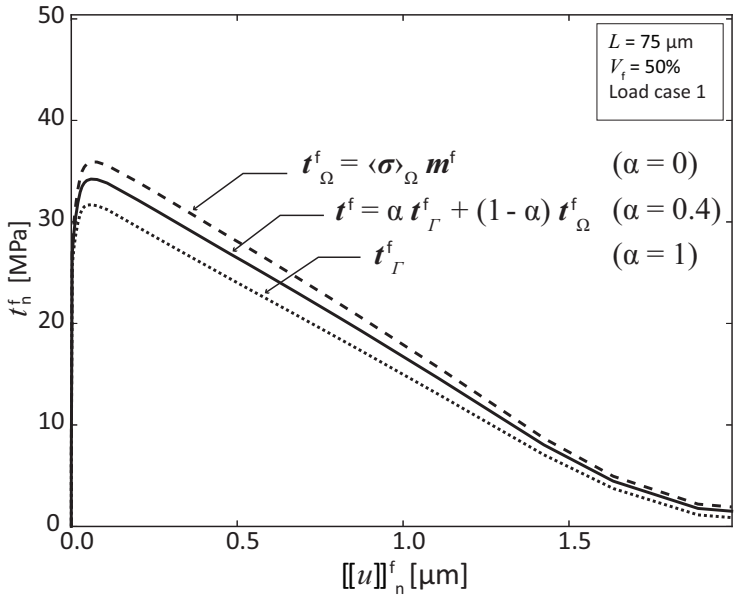

Figure 6: Effective normal traction component as a function of the effective normal crack opening displacement for three values of the weighting parameter α, with $\alpha = 0.4$ being the optimal value in terms of satisfying the Hill-Mandel condition. The curves correspond to a 75μm $\times$ 75μm microscopic volume element under laterally-constrained axial extension.

numerical experimentation, values close to 0 often provide a reasonable match, which suggests that the volume-averaged traction $\boldsymbol{t}^{\mathrm{f}}_{\Omega}$ may be used as a first option to approximate the effective traction $\boldsymbol{t}^{\mathrm{f}}$ in the absence of a detailed analysis as the one presented here. However, optimal values of α close to 1 were not uncommon, which justifies in general a thorough post-processing protocol to verify a posteriori the multiscale approach and establish the proper values for the effective traction.

6. Representative volume elements for various loading cases

6.1. Procedure to establish an RVE

Once it has been verified that the crack-based Hill-Mandel condition can be approximately satisfied with the choice of a weighting factor α, the next step is to verify the existence of a representative volume element (RVE) for fracture in the sense of a (converged) effective traction-separation relation. To this end, a sequence of $L \times L$ microscopic volume elements (MVE) of increasing size are used, namely $L = 12.5$ (unit cell), $37.5, 50, 62.5, 75\mu$m as shown in Fig. 7. Each MVE represents a cross-section perpendicular to the fiber direction of an uni-directional fiber-reinforced composite with randomly-distributed fibers. The so-called unit cell volume element, consisting of a single fiber centered in the computational domain, is a special case since, due to periodicity, it corresponds to a non-random, orthotropic arrangement whereas the other MVEs are meant to represent a transversely isotropic material. All MVEs have nominally the same average composition, which in this case is measured by a fiber volume fraction of 50%. Due to the discrete nature of the volume elements, the actual volume fractions deviate from the nominal value (see Table 2).

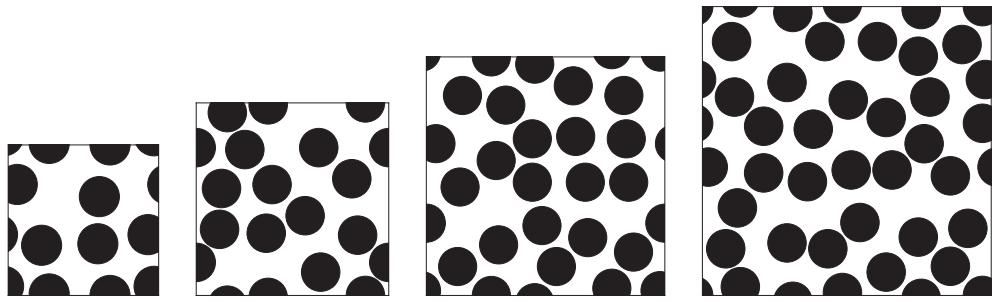

Figure 7: Microscopic volume elements tested in the convergence study to establish a representative volume element, together with a so-called unit cell, not shown here, consisting of a single fiber centered in a $12.5\mu\text{m} \times 12.5\mu\text{m}$ domain.

Table 2: Geometrical characteristics of microscopic volume elements (MVEs). The fiber diameter is 10 μm.

MVE size [μm^2]	Number of fibers	Actual fiber volume fraction [%]
12.5×12.5 (unit cell)	1	50.3
37.5×37.5	8	44.7
50×50	15	47.1
62.5×62.5	24	48.3
75×75	35	48.9

The basic load cases used to test the procedure are given in Table 3. The cases consist of a nominally mode I deformation (load case 1: laterally-constrained axial extension), a nominally mode II deformation (load case 2: equal biaxial extension-contraction corresponding to pure shear) and a mixed-mode deformation (load case 3: mixed extension-simple shear). The displacement gradient of each deformation is indicated in Table 3. For load cases 1 and 2 the displacement gradient is symmetric hence it coincides with the applied strain tensor. For load case 3 the displacement gradient is not symmetric hence the deformation includes a rigid body rotation that can be approximated for infinitesimally small deformations using the skew-symmetric part of the displacement gradient. Simulations for a similar loading condition, namely mixed extension-pure shear without rigid body rotation, provided similar results as load case 3.

For each load case, a convergence analysis regarding the size of the representative volume element was carried out with the volume elements indicated above in Table 2. For each size (except for the unit cell), five realizations with randomly-distributed fibers were generated and the

Table 3: Basic load cases defined in terms of the applied strain (see also Fig. 2 for nomenclature)

Load case	Description	Applied displacement gradient $\nabla \boldsymbol{u}$
1	Laterally-constrained axial extension	$\epsilon_0 \boldsymbol{e}_1 \otimes \boldsymbol{e}_1$
2	Pure shear (equal biaxial extension-contraction)	$\gamma_0(\boldsymbol{e}_1 \otimes \boldsymbol{e}_1 - \boldsymbol{e}_2 \otimes \boldsymbol{e}_2)$
3	Mixed extension-simple shear	$\epsilon_0 \boldsymbol{e}_1 \otimes \boldsymbol{e}_1 + \gamma_0 \boldsymbol{e}_1 \otimes \boldsymbol{e}_2$

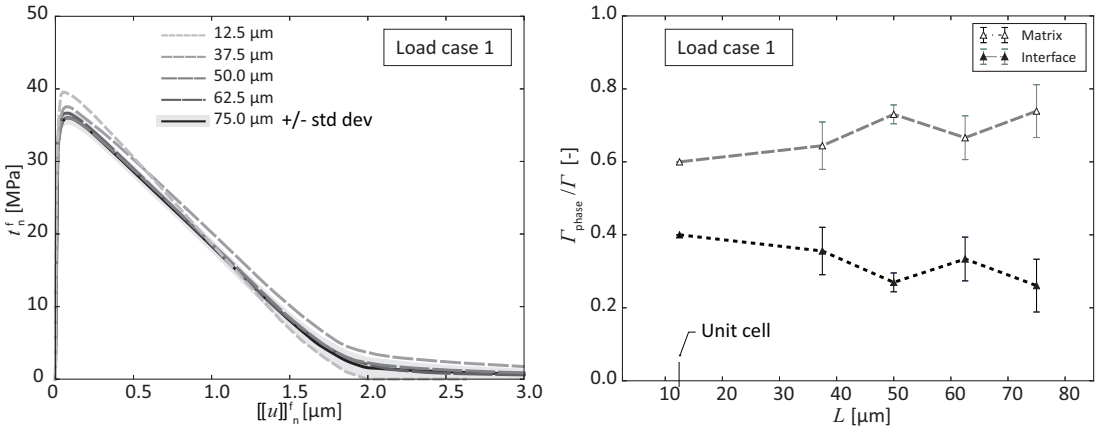

Figure 8: (a) Effective normal traction component as a function of the effective normal crack opening displacement and (b) crack phase partition between matrix and interface for various microscopic volume elements tested under load case 1 (laterally-constrained axial extension). The effective tangential traction component (not shown here) was negligible. No fiber cracking was observed in these simulations.

(discrete) standard deviations and mean values of the responses were computed. In addition, it was verified that for each simulation the appropriate mesh density was used by performing individual mesh convergence analyses (not reported here for conciseness). Mesh convergence was achieved with characteristic element lengths ranging from 0.25μm to 2μm for increasing volume element sizes. In the following sections, the (numerical) existence of a representative volume element is shown for the three loading cases considered.

6.2. RVE for load case 1: laterally-constrained axial extension

A typical volume element loaded under laterally-constrained axial tension (load case 1) is shown in Fig. 4. After postprocessing, the orientation of the equivalent macroscopic crack normal $\boldsymbol{m}^{\mathrm{f}}$ is found to be close to the vector $\boldsymbol{e}_1$ (see Fig. 2 for nomenclature). The effective normal traction $t_{\mathrm{n}}^{\mathrm{f}}$ as a function of the effective normal crack opening displacement $[\![u]\!]_{\mathrm{n}}^{\mathrm{f}}$ is shown in Fig. 8a for the distinct MVEs. The effective tractions were determined using the optimal value of the weighting parameter α for each simulation as described in Sec. 5. The shaded area represents the standard deviation of five realizations (for clarity shown only for the MVE corresponding to $L = 75\mu$m). The crack length partition $|\Gamma_{\mathrm{phase}}|/|\Gamma|$ between matrix cracking and fiber-matrix interface separation is shown in Fig. 8b.

As can be observed in Fig. 8a, the effective traction-separation relation for loading case 1 converges relatively fast as a function of MVE size to within an acceptable tolerance. Even the unit cell simulation, which does not represent a transversely isotropic material, already provides reasonable results in terms of the fracture energy although it overestimates the fracture strength by about 15%. Using a distinct measure of convergence, namely the crack length partition as shown in Fig. 8b, the unit cell predicts that about 60% of the crack runs through fiber-matrix interfaces while 40% runs through the matrix. For the larger MVEs analyzed, the average prediction (based on five realizations per MVE size) is about 70% fiber-matrix interface cracking and about 30%

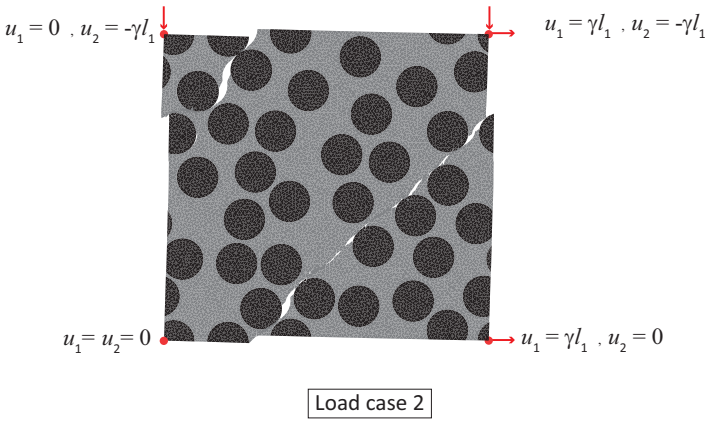

Figure 9: Example of a fully-failed MVE under load case 2 (equal biaxial extension-contraction, corresponding to pure shear)

matrix cracking. From the information shown in Fig. 8 it can be concluded that a reasonable RVE size for load case 1 is $L = 50\mu$m.

6.3. RVE for load case 2: pure shear (equal biaxial extension-contraction)

At a fully-failed state, a typical volume element loaded under pure shear is shown in Fig. 9 (applied as equal biaxial extension-contraction, see loading case 2 in Table 3). For about half of the samples, the orientation of the equivalent macroscopic crack normal $\boldsymbol{m}^{\mathrm{f}}$ is found to be close to the vector $(1/\sqrt{2})(\boldsymbol{e}_1 + \boldsymbol{e}_2)$ while for the other half of the samples the orientation was found to be close to $(1/\sqrt{2})(-\boldsymbol{e}_1 + \boldsymbol{e}_2)$, as in the example shown in Fig. 9. The crack pattern in this case differs from that of load case 1 in the sense that the normal opening is small compared to the tangential opening. The effective tangential traction $t_{\mathrm{s}}^{\mathrm{f}}$ as a function of the effective tangential crack opening displacement $[\![u]\!]_{\mathrm{s}}^{\mathrm{f}}$ is shown in Fig. 10a for the distinct MVEs. As before, the shaded area represents the standard deviation of five realizations, which, for clarity, is shown only for the MVE corresponding to $L = 75\mu$m. The effective normal traction component in this loading case was negligible in comparison to the tangential one. The crack length partition $|\Gamma_{\mathrm{phase}}|/|\Gamma|$ between matrix cracking and fiber-matrix interface separation is shown in Fig. 10b.

From Fig. 10a, it can be observed that the unit cell underestimates the effective fracture strength and fracture energy. Larger MVEs are required to capture sufficient details and interactions in the cracking process to obtain a converged response. In this case, a reasonable convergence is reached with the largest MVE analyzed, namely $L = 75\mu$m. It is interesting to observe that, in terms of the crack partition, all MVEs predict approximately the same values, namely about 50% fiber-matrix interface cracking and 50% matrix cracking. Hence, in contrast to load case 1, the measure of convergence for load case 2 based on morphology (crack partition) is less stringent than the measure of convergence based on effective traction-separation response. Based on the data shown in Fig. 10 it can be concluded that a reasonable RVE size for load case 2 is $L = 75\mu$m.

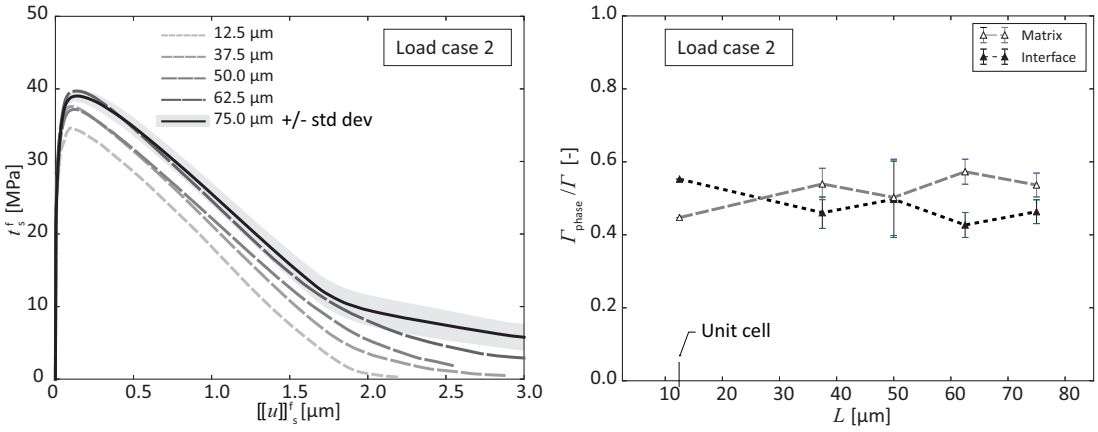

Figure 10: (a) Effective tangential traction component as a function of the effective tangential crack opening displacement and (b) crack phase partition between matrix and interface for various microscopic volume elements tested under load case 2 (equal biaxial extension-contraction, corresponding to pure shear). The effective normal traction component (not shown here) was negligible. No fiber cracking was observed in these simulations.

6.4. RVE for Mixed extension-simple shear

For the mixed mode case (load case 3, composed of extension and simple shear with $\epsilon_0 = \gamma_0 = \gamma$), a typical crack pattern in the volume element is shown in Fig. 11. The main periodic crack is somewhat similar to that of load case 1 except that a branch (crack bifurcation) appears at an inclined angle with respect to the main crack, see Fig. 11). Nevertheless, the contribution of the branch is relatively small and the orientation of the equivalent macroscopic crack normal $\boldsymbol{m}^{\mathrm{f}}$ is found to be close to the vector $\boldsymbol{e}_1$.

Although cases 1 and 3 have a similar crack morphology, the tangential component of the equivalent traction in case 3 is not negligible as shown in Fig. 12 which includes the normal and tangential components of the effective traction as a function of the corresponding normal and tangential components of the effective crack opening for various MVEs (see Fig. 12a and Fig. 12b, respectively). The norm of the effective traction as a function of the norm of the crack opening displacement is given in Fig. 12c and the crack length partition $|\Gamma_{\mathrm{phase}}|/|\Gamma|$ between matrix cracking and interface separation is shown in Fig. 12d.

In this mixed mode loading case, convergence towards an RVE is slower than in the previous loading cases. Although the normal component of the traction shows a reasonable convergence, particularly at the early stages of degradation, the tangential component tends to fluctuate more significantly, only showing a partial convergence. Both components have a relatively wide standard deviation region, particularly at the later stages of degradation for the normal component (see shaded area in figure). In terms of the combined response curve shown in Fig. 12, convergence is only visible until an effective crack opening of about 1 μm, while the last stage shows a greater level of uncertainty. On the other hand, as can be seen based in Fig. 12d, the crack partition predicted by all MVEs is somewhat similar, corresponding to about 70% fiber-matrix interface cracking and 30% matrix cracking. Based on the data shown in Fig. 12 it can be concluded that for load case 3, the largest MVE with $L = 75\mu$m provides a reasonable approximation to an RVE but using a relatively large tolerance.

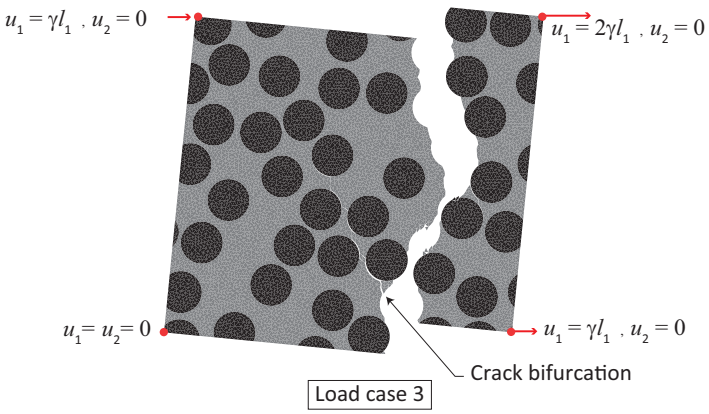

Figure 11: Example of a fully-failed MVE under load case 3 (Mixed extension-simple shear with $\epsilon_0 = \gamma_0 = \gamma$)

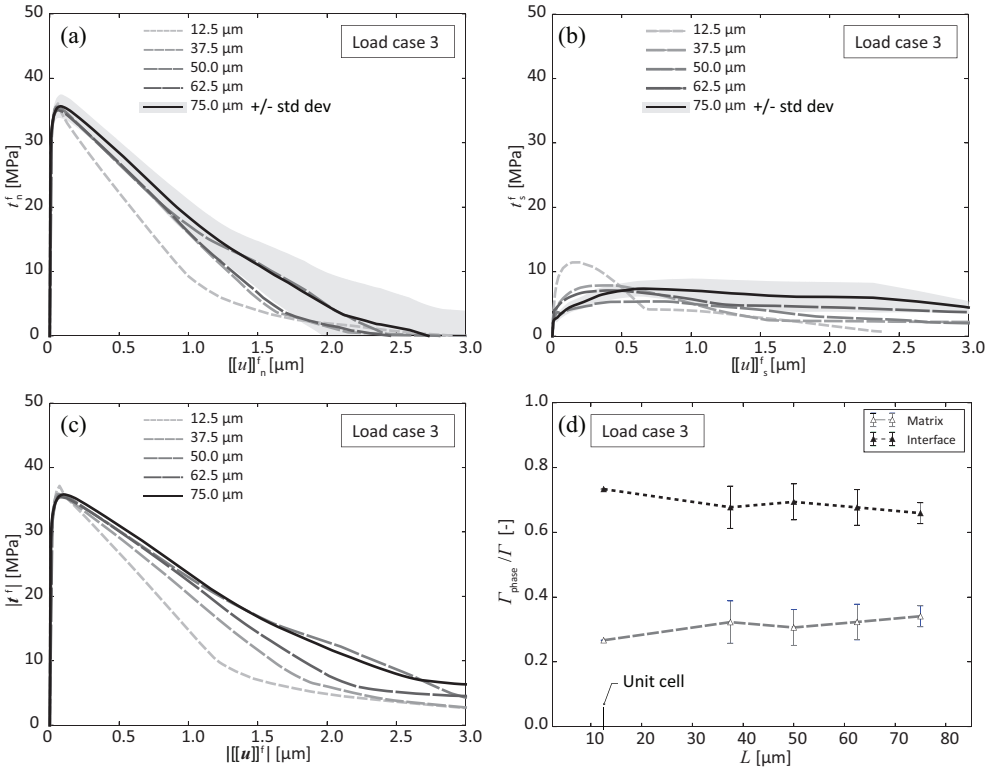

Figure 12: (a) Effective normal traction component as a function of the effective normal crack opening displacement, (b) Effective tangential traction component as a function of the effective tangential crack opening displacement, (c) equivalent traction as a function of the equivalent crack opening displacement and (d) crack phase partition between matrix and interface for various microscopic volume elements tested under load case 3 (mixed extension-simple shear). No fiber cracking was observed in these simulations.

Table 4: Applied strain and corresponding orientation of macroscopic crack (crack normal) and mode mixity at failure based on simulations. Vector components are referred to the global basis as indicated in Fig. 2 and $\epsilon_0 = \gamma_0 = \gamma$ in Table 3

Load case	Description	Principal strains	Principal strain directions (angles w.r.t $\boldsymbol{e}_1$)	Crack normal(s) (angles w.r.t $\boldsymbol{e}_1$)	mode mixity at failure (in rad)
1	Axial extension	$\gamma; 0$	$0°; 90°$	$0°$	0.01
2	Pure shear	$\pm\gamma$	$0°; 90°$	$\pm 45°$	1.44
3	Mixed loading	$(1 \pm \sqrt{2})\gamma/2$	$22.5°; 112.5°$	$0°$	0.69

7. Effective nucleation criterion and traction-separation relation

The methodology developed in the present work may be applied systematically in order to generate microscale-based information to propose and/or calibrate an effective (macroscale) nucleation criterion and an effective traction separation relation that capture, on average, the microscopic behavior as described in Sec. 4.3. For the type of MVEs analyzed in the present work, the macroscopic scale refers to a ply in a laminate where the interactions between fiber, matrix and interfaces have been homogenized into a single model. In particular, an effective nucleation criterion may be proposed and calibrated for each loading case in order to predict the orientation of a macroscopic crack (see (28)) and the corresponding traction-separation relation may be obtained from postprocessing. Subsequently, the calibrated responses for the loading cases may be combined into a single model. The calibration step is outside of the scope of the present work, but it is worth summarizing the results of the three load cases from Sec. 6. To this end, the mode-mixity parameter β is defined as follows:

$$\beta := \arctan \frac{[\![u]\!]^{\mathrm{f}}_{\mathrm{s}}}{[\![u]\!]^{\mathrm{f}}_{\mathrm{n}}}$$

where the subscripts n and s refer to the normal and tangential components of the effective crack opening. Typically, the mode mixity varies throughout the simulation. To simplify the calibration process, it is convenient to define a nominal mode mixity parameter β_F, which may be also termed the mode mixity at final failure, as

$$\beta_F := \arctan \frac{[\![u]\!]^{\mathrm{f}}_{\mathrm{s},F}}{[\![u]\!]^{\mathrm{f}}_{\mathrm{n},F}}$$

where the additional subscript F indicates the state at final failure, i.e., the vector $[\![\boldsymbol{u}]\!]^{\mathrm{f}}_F$ represents the effective crack opening at time $t = t_F$. The results of the three loading cases analyzed are reported in Table 4, which indicates the principal strains and principal directions of the applied strain (eigenvectors associated to the applied strain under proportional loading), the macroscopic crack normal vector $\boldsymbol{m}^{\mathrm{f}}$ and the mode mixity at failure as obtained from the post-processing of the simulation data. As may be observed from the table, the first loading case is close to a nominal mode I loading ($\beta_F \approx 0$) while the second loading case is close to a nominal mode II loading ($\beta_F \approx \pi/2$). Observe that in terms of the orientation of the crack normal $\boldsymbol{m}^{\mathrm{f}}$, case 1 follows a

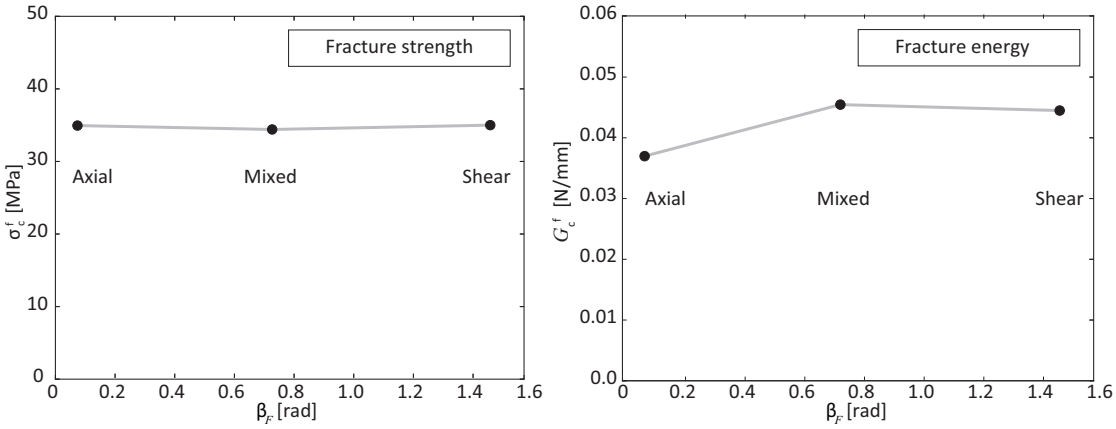

Figure 13: (a) Effective equivalent fracture strength and (b) Effective equivalent fracture energy as a function of a mode-mixity parameter.

classical maximum principal strain failure criterion, case 2 follows a maximum shear strain failure criterion and the mixed mode case 3 contains ingredients of both cases. In terms of an effective traction-separation relation, the effective equivalent fracture strength σ_c^f and the effective equivalent fracture energy G_c^f are given, respectively, in Fig. 13a and Fig. 13b as a function of the mode mixity at failure. The lines connecting the three load cases are only provided for visual reference and should not be directly used for interpolation, which requires a more extensive analysis with sufficient loading cases. Nevertheless, it may be observed that the predicted fracture strength is approximately constant for all three loading cases. The fracture energy for mode II and the mixed mode case are similar and about 17% higher than the fracture energy for mode I, albeit with a relatively large uncertainty for the mixed mode.

In principle one may use a simple bilinear traction-separation relation at the macroscopic level for which the above-mentioned values are sufficient in terms of calibration, in conjunction with a curve fitting using the parameter β_F as a variable. If it is required to carry over more details from the microscale to the effective traction-separation relation at the macroscale, other relations such as trilinear or exponential functions may be used as well with the corresponding curve fitting procedure.

8. Concluding remarks

The present work summarizes a multiscale procedure to derive an effective nucleation criterion and an effective traction-separation relation at the macroscale based on microscale simulations of representative volume elements. It is shown that the simulations can be performed using periodic boundary conditions that allow cracks to propagate across the volume boundaries in arbitrary directions. A relevant finding in the analysis of the scale transition requirements is that, in addition to the classical "global" Hill-Mandel condition that applies to the whole computational domain, a separate crack-based Hill-Mandel condition needs to be satisfied. The methodology proposed here is to satisfy a priori the global condition using periodic boundary conditions while the crack-based condition is satisfied a posteriori using a weighting parameter to identify the effective traction

acting on the macroscopic crack. In this fashion, parametric simulations with distinct loading cases may be used to generate sufficient data to calibrate an effective (macroscale) constitutive model for fracture. In turn, the effective model may be used in a classical (single-scale) simulation while implicitly incorporating the microscale behavior of a composite material.

Examples shown in the present work pertain to microscale (sub-ply) simulations of an unidirectional reinforced composite. For simplicity the simulations are limited to cross-sections perpendicular to the fiber direction. Simulations with cross-sections along the fiber directions, not shown here, indicate that the theory developed in the present work needs to be extended to account for anisotropic effects. Moreover, simulations of purely-compressive load cases require an extension of the cohesive zone method to account for contact in crushing zones, which is however outside of the present scope. Finally, it is worth pointing out that the method pertains to a hierarchical multiscale analysis in all space directions; in situations where the RVE exceeds the thickness of a ply, a straightforward modification can be applied to modify the crack propagation behavior at the ply interface while retaining the rest of the implementation. Despite the aforementioned limitations and challenges, the current framework is a step in the direction of a multiscale analysis of fracture that accounts for dissipation in a consistent way through the crack-based Hill-Mandel condition.

Appendix A. Periodic Crack

The domain Ω can be deformed until complete failure (i.e., zero load) based on the imposed strain history $\overline{\boldsymbol{\epsilon}} = \overline{\boldsymbol{\epsilon}}(t)$. At complete failure there may be several crack segments that represent periodic cracks, crack branches, or isolated segments. A proper interpretation of the microscale crack (i.e., Γ) in terms of these segments is important. This appendix contains a procedure to identify a periodic crack and a region that completely surrounds it based solely on information from the original domain Ω.

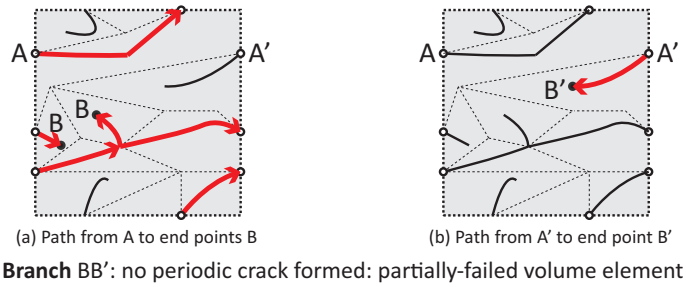

Figure A.14: Identification of periodic cracks, crack branches, or isolated segments: (a) Inward path from A to end points B, (b) Inward path from A' to end points B'. The crack in the domain corresponds to an isolated crack BB', hence there is no periodic crack formed yet in which case the volume element has not fully-failed and may still carry loads.

A crack segment may leave and re-enter the domain multiple times (see Fig. A.14). These crossings of the external boundary always occur in periodically-equivalent entry/exit points (e.g., points A and A') due to the Periodic Boundary Conditions (PBCs). At each of these points it is possible to follow the crack path in two directions (i.e., paths AB and $A'B'$). While doing this

three crack types can be identified, which is illustrated by a partially-failed domain (Fig. A.14) and a domain containing a periodic crack (Fig. A.15). A *periodic macrocrack* is formed if the end point of a path coincides with the periodically-equivalent initial point, see path AA' in Fig. A.15a. A *crack branch* is defined as a separate path from a bifurcation point. An *isolated crack* is not connected to either the periodic crack or crack branches, see Fig. A.15b.

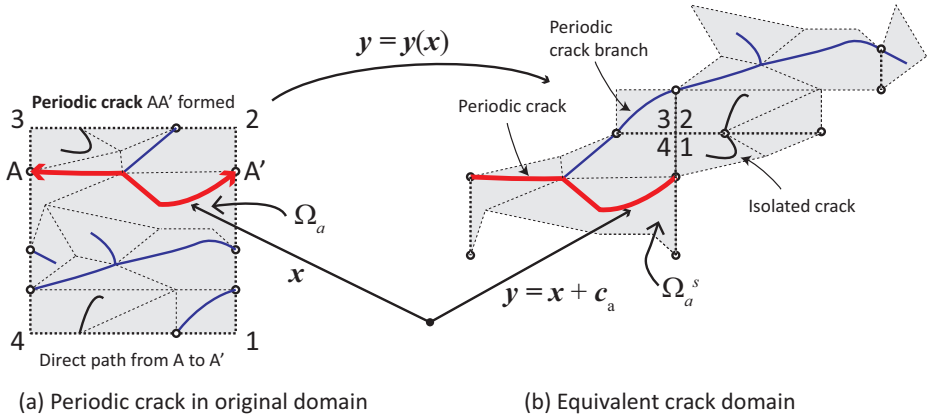

Figure A.15: Identification of the periodic cracks, branches, or isolated segments: (a) Formation of a periodic crack AA', (b) Visualization of periodic crack and surrounding material, termed the equivalent crack domain Ω^s, which can be reconstructed from the original domain with the shifting mapping $\boldsymbol{y} = \boldsymbol{y}(\boldsymbol{x})$.

For visualization purposes it is useful to construct a new domain that fully encompasses these three crack types. The original domain Ω can be divided into subdomains (Ω_a, with $a = 1, \ldots, N$), as shown in Fig. A.15. A new *equivalent crack domain* Ω^s is constructed by "shifting" the subdomains such that their boundaries $\partial\Omega^s$ do not contain finite segments of Γ. The main objective is to assure that the macrocrack is fully-contained inside this new domain. Fig. A.15b illustrates the result of this operation. The corresponding translation of the original crack surface Γ is termed the *equivalent crack surface* Γ^s. A generic point $\boldsymbol{y}$ in Ω^s_a is obtained through adding a translation vector $\boldsymbol{c}_a$ to the original point $\boldsymbol{x}$ in Ω_a,

$$\boldsymbol{y} = \boldsymbol{y}(\boldsymbol{x}) = \boldsymbol{x} + \boldsymbol{c}_a \qquad \boldsymbol{c}_a := N_1^a l_1 \boldsymbol{n}_1 + N_2^a l_2 \boldsymbol{n}_2 \quad \boldsymbol{x} \in \Omega_a \quad a = 1, \ldots, N \tag{A.1}$$

where N_1^a and N_b^a are integer numbers associated to the number of unit translations required to map the original subdomain Ω_a into Ω^s_a in either the $\pm\boldsymbol{n}_1$ and/or $\pm\boldsymbol{n}_2$ directions.

The next step is to establish a relation between integrals in Ω^s, $\partial\Omega^s$, and Γ^s in terms of integrals in Ω, $\partial\Omega$ and Γ. All Jacobians in the integrals are equal to 1 since a rigid body translation does not affect lengths or orientations. As a result, integrals in the equivalent crack domain, of quantities that are insensitive to piecewise constant rigid body translations, are essentially the same as in the original domain. Since the strain and stress tensors are insensitive to rigid body translations, it follows that

$$\langle \boldsymbol{\sigma} \rangle_{\Omega^s} = \langle \boldsymbol{\sigma} \rangle_{\Omega}\,, \qquad \langle \boldsymbol{\epsilon} \rangle_{\Omega^s} = \langle \boldsymbol{\epsilon} \rangle_{\Omega}\,,$$

Further, the displacement jump and the crack normal vector are unaffected by a rigid body translation, since the subdomains fully contain individual crack segments. Consequently,

$$\boldsymbol{\epsilon}^{\mathrm{f}}_{\Omega^s} = \boldsymbol{\epsilon}^{\mathrm{f}}$$

with $\boldsymbol{\epsilon}^{\mathrm{f}}$ being the fracture strain computed in Ω.

The previous relations can simply be established by inspection. However, this may not be obvious for the surface integral of the field $[\boldsymbol{u} \otimes \boldsymbol{n}]_{\mathrm{sym}}$ on $\partial\Omega$, which may be different than the surface integral of the equivalent field on $\partial\Omega^{\mathrm{s}}$ since the displacement field is sensitive to piecewise constant translations. Below it is shown that these two quantities are equal. To prove this, consider the previously-derived expression for the applied macroscopic strain in Ω, which can be written as

$$\bar{\boldsymbol{\epsilon}} = \frac{1}{|\Omega|} \int_{\partial\Omega} [\boldsymbol{u}(\boldsymbol{x}) \otimes \boldsymbol{n}(\boldsymbol{x})]_{\mathrm{sym}} \, \mathrm{d}s = \frac{1}{|\Omega|} \sum_{a=1}^{N} \int_{\partial\Omega_a} [\boldsymbol{u}(\boldsymbol{x}) \otimes \boldsymbol{n}(\boldsymbol{x})]_{\mathrm{sym}} \, \mathrm{d}s \, ,$$

where the vector field $\boldsymbol{n}$ has been extended to include the normal vectors of the internal boundaries of the subdomains Ω_a. The net contributions of the integrals along the boundaries of subdomains Ω_a is zero due to the continuity of the displacement across those boundaries. The actual macroscopic strain $\bar{\boldsymbol{\epsilon}}^{\mathrm{s}}$ applied in Ω^{s} after shifting is

$$\bar{\boldsymbol{\epsilon}}^{\mathrm{s}} := \frac{1}{|\Omega^{\mathrm{s}}|} \sum_{a=1}^{N} \int_{\partial\Omega_a^{\mathrm{s}}} [\boldsymbol{u}(\boldsymbol{y}) \otimes \boldsymbol{n}(\boldsymbol{y})]_{\mathrm{sym}} \, \mathrm{d}s \tag{A.2}$$

where $\boldsymbol{u}(\boldsymbol{y})$ refers to the actual displacement at point $\boldsymbol{y}$, which is continuous across the boundaries $\partial\Omega_a^{\mathrm{s}}$ that lie in the interior of Ω_a^{s}. Since the normal vector $\boldsymbol{n}$ is insensitive to the shifting operation it can be concluded that $\boldsymbol{n}(\boldsymbol{y}) = \boldsymbol{n}(\boldsymbol{x})$. The relation between the displacements at $\boldsymbol{y}$ and $\boldsymbol{x}$ is expressed in terms of the applied macroscopic strain and the corresponding translation vector given in Eq. A.1,

$$\boldsymbol{u}(\boldsymbol{y}) = \boldsymbol{u}(\boldsymbol{x}) + \bar{\boldsymbol{\epsilon}}\boldsymbol{c}_a \qquad \boldsymbol{y} \in \Omega_a^{\mathrm{s}} \quad \boldsymbol{x} \in \Omega_a \quad a = 1, \ldots, N \, .$$

Substituting this relation in Eq. A.2 and changing variables of integration (i.e., $|\Omega^{\mathrm{s}}| = |\Omega|$) gives

$$\bar{\boldsymbol{\epsilon}}^{\mathrm{s}} = \frac{1}{|\Omega^{\mathrm{s}}|} \sum_{a=1}^{N} \int_{\partial\Omega_a^{\mathrm{s}}} [\boldsymbol{u}(\boldsymbol{y}) \otimes \boldsymbol{n}(\boldsymbol{y})]_{\mathrm{sym}} \, \mathrm{d}s = \frac{1}{|\Omega|} \sum_{a=1}^{N} \int_{\partial\Omega_a} [(\boldsymbol{u}(\boldsymbol{x}) + \bar{\boldsymbol{\epsilon}}\boldsymbol{c}_a) \otimes \boldsymbol{n}(\boldsymbol{x})]_{\mathrm{sym}} \, \mathrm{d}s \, ,$$

which, from the properties of the symmetric tensor $\bar{\boldsymbol{\epsilon}}$, can be further expressed as

$$\bar{\boldsymbol{\epsilon}}^{\mathrm{s}} = \bar{\boldsymbol{\epsilon}} + \left(\frac{1}{|\Omega|} \sum_{a=1}^{N} \int_{\partial\Omega_a} [\boldsymbol{c}_a \otimes \boldsymbol{n}]_{\mathrm{sym}} \, \mathrm{d}s \right) \bar{\boldsymbol{\epsilon}} = \bar{\boldsymbol{\epsilon}} + \left(\frac{1}{|\Omega|} \sum_{a=1}^{N} \left[\boldsymbol{c}_a \otimes \int_{\partial\Omega_a} \boldsymbol{n} \mathrm{d}s \right]_{\mathrm{sym}} \right) \bar{\boldsymbol{\epsilon}} \, .$$

The term in parentheses is zero since every integral is zero on the (closed) boundary of each subdomain Ω_a. Hence, the externally applied macrostrain $\bar{\boldsymbol{\epsilon}}$ on Ω, coincides with the macrostrain $\bar{\boldsymbol{\epsilon}}^{\mathrm{s}}$ applied in Ω^{s},

$$\bar{\boldsymbol{\epsilon}}^{\mathrm{s}} = \bar{\boldsymbol{\epsilon}} \, . \tag{A.3}$$

The above shows that the PBCs apply to the same periodic crack (with possibly several branches and/or isolated segments) and that the response is unaffected by adjacent (parallel) periodic cracks. Hence, a multiscale analysis for fracture may be carried out with PBCs. The PBCs and the orientation (or shape) of the computational domain do not constrain the nucleation and orientations of

cracks, which are allowed to appear at arbitrary locations and in arbitrary directions. The advantage of PBCs is that they are relatively simple to implement numerically.

However, care must be exercised interpreting the results in Ω. A commonly-used method to impose the macroscopic strain is to specify the displacement of master nodes (i.e., corner nodes $\boldsymbol{x}^{(i)}$ or fictitious nodes). The corner nodes may be separated by more than one parallel macrocrack, in which case the strain $\overline{\boldsymbol{\epsilon}}$ acts on *multiple* (but otherwise *identical*) parallel cracks. In addition, a situation can arise where two (or more) distinct periodic cracks coalesce in the domain in the case the applied strain can still be (partially) carried out after the formation of one periodic crack. An equivalent crack domain in this case, which would include one crossing point between two periodic cracks, is still applicable since the shifting mapping given in Eq. A.1 does not distinguish between one or multiple periodic cracks. However, the methodology developed in the Sec. 4 is intended for a single equivalent macrocrack. It can be extended to treat the case of bifurcations but that analysis is beyond the scope of the present work.

References

I. M. Gitman, H. Askes, L. J. Sluys, Representative volume: Existence and size determination, Engineering Fracture Mechanics 74 (16) (2007) 2518–2534.

V. P. Nguyen, O. Lloberas-Valls, M. Stroeven, L. J. Sluys, On the existence of representative volumes for softening quasi-brittle materials - A failure zone averaging scheme, Computer Methods in Applied Mechanics and Engineering 199 (45-48) (2010) 3028–3038.

C. V. Verhoosel, J. J. C. Remmers, M. A. Gutierrez, R. de Borst, Computational homogenization for adhesive and cohesive failure in quasi-brittle solids, International Journal for Numerical Methods in Engineering 83 (8-9, SI) (2010) 1155–1179, ISSN 0029-5981.

K. Matous, M. G. Kulkarni, P. H. Geubelle, Multiscale cohesive failure modeling of heterogeneous adhesives, Journal of the Mechanics and Physics of Solids 56 (4) (2008) 1511–1533.

M. G. Kulkarni, K. Matous, P. H. Geubelle, Coupled multi-scale cohesive modeling of failure in heterogeneous adhesives, International Journal for Numerical Methods in Engineering 84 (8) (2010) 916–946.

A. R. Melro, P. P. Camanho, F. M. Andrade Pires, S. T. Pinho, Micromechanical analysis of polymer composites reinforced by unidirectional fibres: Part I - Constitutive modelling, International Journal of Solids and Structures 50 (11-12) (2013) 1897–1905.

M. V. C. Alfaro, A. S. J. Suiker, C. V. Verhoosel, R. de Borst, Numerical homogenization of cracking processes in thin fibre-epoxy layers, European Journal of Mechanics A-Solids 29 (2) (2010a) 119–131.

A. Arteiro, G. Catalanotti, A. R. Melro, P. Linde, P. P. Camanho, Micro-mechanical analysis of the in situ effect in polymer composite laminates, Composite Structures 116 (1) (2014) 827–840, ISSN 02638223, URL `http://dx.doi.org/10.1016/j.compstruct.2014.06.014`.

E. W. C. Coenen, V. G. Kouznetsova, M. G. D. Geers, Novel boundary conditions for strain localization analyses in microstructural volume elements, International Journal for Numerical Methods in Engineering 90 (1) (2012a) 1–21.

E. W. C. Coenen, V. G. Kouznetsova, E. Bosco, M. G. D. Geers, A multi-scale approach to bridge microscale damage and macroscale failure: a nested computational homogenization-localization framework, International Journal of Fracture 178 (1-2, SI) (2012b) 157–178, ISSN 0376-9429.

E. Bosco, V. G. Kouznetsova, M. G. D. Geers, Multi-scale computational homogenization-localization for propagating discontinuities using X-FEM, International Journal for Numerical Methods in Engineering 102 (3-4, SI) (2015) 496–527.

E. Svenning, M. Fagerström, F. Larsson, Computational homogenization of microfractured continua using weakly periodic boundary conditions, Computer Methods in Applied Mechanics and Engineering 299 (2016a) 1–21, ISSN 00457825.

E. Svenning, M. Fagerstrom, F. Larsson, On computational homogenization of microscale crack propagation, International Journal for Numerical Methods in Engineering 108 (1) (2016b) 76–90.
M. Mosby, K. Matous, Computational homogenization at extreme scales, Extreme Mechanics Letters 6 (2016) 68–74, ISSN 2352-4316.
R. Hill, Constitutive macro-variables for heterogeneous solids at finite strain, Proceedings of the Royal Society of London Series A-Mathematical and Physical Sciences 326 (1565) (1972) 131–&.
R. Hill, On the micro-to-macro transition in constitutive analyses of elastoplastic response at finite strain, Mathematical Proceedings of the Cambridge Philosophical Society 98 (NOV) (1985) 579–590.
J. F. Unger, An FE2-X1 approach for multiscale localization phenomena, Journal of the Mechanics and Physics of Solids 61 (4) (2013) 928–948, ISSN 00225096.
S. A. Ponnusami, S. Turteltaub, S. van der Zwaag, Cohesive-zone modelling of crack nucleation and propagation in particulate composites, Engineering Fracture Mechanics 149 (2015) 170–190, ISSN 0013-7944.
W. Westbroek, Multiscale Modeling of Fracture in Composites: A Progressive Failure Model for Cryogenic Applications, Master's thesis, Delft University of Technology, 2017.
T. S. Hille, A. S. J. Suiker, S. Turteltaub, Microcrack nucleation in thermal barrier coating systems, Engineering Fracture Mechanics 76 (6, SI) (2009) 813–825, ISSN 0013-7944.
N. van Hoorn, Multiscale fracture simulations for composite materials, Master's thesis, Delft University of Technology, 2016.
M. V. C. Alfaro, A. S. J. Suiker, R. de Borst, Transverse Failure Behavior of Fiber-epoxy Systems, Journal of Composite Materials 44 (12) (2010b) 1493–1516.
T. Hobbiebrunken, M. Hojo, T. Adachi, C. De Jong, B. Fiedler, Evaluation of interfacial strength in CF/epoxies using FEM and in-situ experiments, Composites Part A-Applied Science and Manufacturing 37 (12, SI) (2006) 2248–2256.